Measurement 134 (2019) 548–568

Contents lists available at ScienceDirect

Measurement

journal homepage: www.elsevier.com/locate/measurement

Structural health monitoring by a new hybrid feature extraction and dynamic time warping methods under ambient vibration and non-stationary signals

Alireza Entezami, Hashem Shariatmadar *

Department of Civil Engineering, Faculty of Engineering, Ferdowsi University of Mashhad, Mashhad, Iran

ARTICLE INFO

Article history:
Received 10 October 2017
Received in revised form 24 October 2018
Accepted 28 October 2018
Available online 29 October 2018

Keywords:
Structural health monitoring
Ambient vibration
Non-stationary signal
Ensemble empirical mode decomposition
Time series analysis
Dynamic time warping

ABSTRACT

Feature extraction and classification are crucial steps of a data-driven structural health monitoring strategy. One of the major issues in feature extraction is to extract damage-sensitive features from non-stationary signals under unknown ambient vibration. Furthermore, the use of high-dimensional features in damage detection is the other challenging issue, which may make a difficult and time-consuming process. This article is initially intended to propose a hybrid algorithm as a combination of EEMD technique and ARARX model for feature extraction. Subsequently, correlation-based dynamic time warping method is proposed to detect damage by using randomly high-dimensional multivariate features. Due to the importance of damage localization, dynamic time warping is eventually applied to locate damage. Experimental datasets of the IASC-ASCE benchmark structure are utilized to validate the accuracy of proposed methods. Results suggest that the proposed methods are effective tools for damage detection and localization under ambient vibration and non-stationary and/or stationary signals.

1. Introduction

Structural health monitoring (SHM) is a vital strategy for civil, mechanical, and aerospace engineering systems due to preventing any irreparable deterioration and damage, reducing maintenance costs, improving dynamic performance, and increasing structural safety and integrity [1]. This strategy includes the equipment of structures with sensors (i.e. accelerometers, strain gages, fiber optics, etc.), measurement of vibration responses (i.e. displacement, strain, acceleration, etc.), extraction of meaningful and significant features from the measured vibration signals, and feature classification for early damage detection, localization, and quantification [2].

Damage is inherently a local phenomenon; hence, a basic requirement for an SHM scheme is to install and distribute a dense sensor network throughout the structure for capturing entire information about the structural dynamics. Due to major advances and new development of sensor technology, the collection of vibration data for SHM applications is no longer a significant topic. The application of non-expensive sensors along with modern data acquisition systems provides an opportunity to use ambient vibrations such as wind, traffic, human activity, etc. for the excitation of engineering systems, particularly civil engineering structures [3]. The great advantage of the ambient vibrations against the forced vibrations is the lack of using expensive and heavy devices for exciting structures, which leads to an efficient and cost-effective SHM program [4]. Under such circumstances, the primary and demanding task is to adopt robust signal processing methods for analyzing measured vibration data and extracting damage-sensitive features (DSFs) [5].

Despite numerous research efforts along with successful results in SHM applications, there are still some challenging issues and limitations. Conventional signal processing techniques in time or frequency domains assume that the measured vibration signals are stationary and linear [6]. However, this assumption may not be accurate resulting from measuring non-stationary vibration signals from the ambient excitations, intrinsic dynamic nature, high-speed mechanical systems, and structural damage or mechanical faults [7–9]. An efficient way for extracting the DSFs from the non-stationary signals is to use adaptive time-frequency data analysis methods [6]. For the first time, Huang et al. [10] proposed empirical mode decomposition (EMD) method to decompose a non-stationary signal into several stationary data named as intrinsic mode functions (IMFs). In order to deal with the major drawback of EMD called mode mixing, Wu and Huang [11] presented a noise-assisted data analysis method known as ensemble

* Corresponding author.
E-mail addresses: entezami@mail.um.ac.ir (A. Entezami), shariatmadar@um.ac.ir (H. Shariatmadar).

https://doi.org/10.1016/j.measurement.2018.10.095
0263-2241/

empirical mode decomposition (EEMD). Due to its great ability to analyze a broad range of stationary and non-stationary signals without the mode mixing problem, the EEMD method has widely been utilized in civil and mechanical systems for damage detection and fault diagnosis [12–17].

In addition, the other significant issue in the context of SHM is concerned with the fact that the ambient vibrations are unmeasurable and unknown [18]. In such cases, one of the efficient and reliable ways for extracting significant DSFs is to model the measured vibration responses acquired from the ambient excitations by parametric time series models such as autoregressive (AR) [19,20], autoregressive with eXogenous input (ARX) [21], autoregressive moving average (ARMA) [18,22], and autoregressive-autoregressive with eXogenous input (ARARX) [23]. The key benefit of using time series modeling for feature extraction is that this process does not depend on the type of excitation sources. Furthermore, the main statistical characteristics of the above-mentioned time series models (i.e. the coefficients and residuals) are sensitive to damage [24]. However, the main premise of using these models is that the vibration time-domain responses should be stationary [25]. In other words, these are not suitable for use in cases that the measured vibration signals are non-stationary. As a result, one robust approach to feature extraction under ambient vibration and non-stationary signals is to utilize a hybrid algorithm as a combination of a time-frequency data analysis technique and a time-invariant linear model.

Apart from the step of feature extraction in the data-driven SHM strategy, the use of high-dimensional time series features is a demanding problem, which may not only make a difficult and time-consuming feature classification process but also provide inaccurate damage detection results, particularly from a dense sensor network [26]. Although dimensionality reduction methods are usually applied to map such features onto a new reduced space, one can alternatively use influential dissimilarity-based or time-series classification methods [27]. The advantage of such methods is the possibility of direct classification of time series features without dimensionality reduction or any concern about the loss of information.

In this article, a new hybrid algorithm for feature extraction is proposed to deal with the significant problem of extracting DSFs from non-stationary vibration signals under ambient vibrations. This algorithm is a combination of the EEMD method and ARARX model named as EEMD-ARARX. On this basis, an IMF with the highest level of energy is initially chosen among all modes extracted from the EEMD technique. Fitting an ARARX model to this IMF, the AR coefficients and ARX residuals are extracted as the most significant DSFs. The major limitation of applying the ARX residuals is that these are randomly high-dimensional multivariate data. Correlation-based dynamic time warping (CDTW) method is proposed to handle this limitation and detect early damage. This approach is based on the segmentation of time series data sets by principal component analysis (PAC)-based techniques and calculation of CDTW dissimilarity quantity using PCA similarity factor. Dynamic time warping (DTW) method is used to locate damage with the aid of the AR coefficients along with a well-known threshold limit. The process of damage localization relies on finding the sensor location associated with the largest DTW value that exceeds the threshold limit. The accuracy and efficiency of the proposed methods are experimentally verified by the IASC-ASCE benchmark structure equipped with a relatively dense sensor network. Results demonstrate that the EEMD-ARARX algorithm succeeds in extracting the significant DSFs from the non-stationary and/or stationary vibration signal under ambient vibrations. Moreover, it will be observed that both CDTW and DTW methods are influentially capable of detecting early damage and identifying the locations of single and multiple damage cases.

The rest of this article is arranged as follows. Section 2 briefly describes the adaptive time-frequency data analysis methods such as EMD and EEMD. Time series analysis by ARARX model is discussed in Section 3. Section 4 presents the proposed EEMD-ARARX algorithm for feature extraction. In Section 5, the time-series classification methods such as CDTW and DTW are explained for the early damage detection and localization. Experimental validation by the IASC-ASCE benchmark structure is evaluated in Section 6. Eventually, Section 7 summarizes the main conclusions regarding this research study.

2. Adaptive time-frequency data analysis methods

2.1. EMD

The EMD is a self-adaptive method that offers an iterative numerical approximate algorithm (sifting process) for the analysis of stationary, non-stationary, and transient signals [10]. This method is based on the decomposition of a signal into a set of complete and almost orthogonal components known as intrinsic mode functions (IMFs). These components arrange from high to low frequencies based on local characteristic timescales. The IMFs indicate the natural vibration mode embedded in the signal and serve as the basis functions determined by the signal itself. This great advantage makes the EMD as an adaptive non-parametric time-frequency analysis approach, which increases its applicability to a wide range of signals without constructing any basis to match the signal characteristic structure [7]. Given a vibration signal in time domain $x(t)$, the process of signal decomposition through the EMD method is given by:

$$x(t) = \sum_{i=1}^{n} c_i(t) + r_n(t) \tag{1}$$

where $c_i(t)$ and $r_n(t)$ represent the i^{th} IMF and the residual (trend) of the original signal, respectively. Each IMF should satisfy two conditions including (i) the numbers of extreme and zero-crossings should differ by not more than one, and (ii) the mean value of envelop defined by the maxima and minima at any given time should be zero. In the following, the algorithm of EMD is summarized as:

1. Initialize: $r_0 = x(t)$ and $i = 1$
2. Extract the i^{th} IMF: c_i
   - 2a. Initialize: $h_{i(k-1)}=r_{i-1}$, $k = 1$
   - 2b. Extract the local maxima and minima of $h_{i(k-1)}$
   - 2c. Interpolate the local maxima and minima by cubic spline lines to form upper and lower envelops of $h_{i(k-1)}$
   - 2d. Calculate the mean $m_{i(k-1)}$ of the upper and lower envelops of $h_{i(k-1)}$
   - 2e. Set $h_{ik} = h_{i(k-1)} - m_{(k-1)}$
   - 2f. If h_{ik} is an IMF then set $c_i = h_{ik}$, else return to step **2b** with $k = k + 1$
3. Define the remainder $r_{i+1} = r_i - c_i$
4. If r_{i+1} still has least two extreme then return to step **2** with $i = i + 1$, else the process of signal decomposition is terminated and r_{i+1} is the residual of the signal

2.2. EEMD

Although the EMD is an effective way in resolving the time-varying structure of signal components, it suffers from the major drawback of mode mixing. The precise definition of mode mixing is that different modes of oscillation appear in one IMF or one mode spread across different IMFs [11]. When the mode mixing occurs, an IMF can cease to have physical meaning by itself due to the presence of different physical processes with different energy levels in a mode. This problem also implies that there is energy leakage from one IMF component to its adjacent mode. On the other hand, the inherent orthogonality characteristic of IMFs is no longer satisfied; therefore, the independence among the decomposed components is not imposed [14]. Under such circumstances, the EMD method cannot extract reliable DSFs because of the problem of mode mixing.

To cope with this important drawback, the EEMD enhances the EMD algorithm to reconstruct better IMFs by adding zero mean unit variance white noise with a limited amplitude (A_n) and a specific ensemble number (N_E) [11]. More precisely, the added white noise uniformly populates the whole time-frequency space leading to components of different scales. During adding this uniformly distributed white noise, the components in different scales of the original signal are automatically projected onto appropriate scales. Since the white noise is added throughout the entire signal decomposition process, no missing scales are available, which lead to the elimination of mode mixing. In addition, the zero mean of the white noise help to cancel out the added white noise in the final ensemble mean, if there are adequate ensemble numbers. This means that the only signal itself remains in the final decomposition result [6,12]. Similar to the EMD method, assume that $x(t)$ is an original vibration signal, which is innocuously populated by a white noise signal $w(t)$ as follows:

$$x_j(t) = x(t) + w_j(t), \qquad j = 1, 2, \ldots, N_E \tag{2}$$

where N_E denotes the number of the ensemble (trail) and $x_j(t)$ is the noise-added signal in the j^{th} trail. Inspired by the EMD algorithm, this signal is decomposed into a series of IMFs in the following form:

$$x_j(t) = \sum_{i=1}^{n_j} c_{i,j}(t) + r_{n_j}(t), \qquad j = 1, 2, \ldots, N_E \tag{3}$$

where $c_{i,j}$ represents the i^{th} IMF of the j^{th} ensemble, r_{nj} is the residual of j^{th} ensemble and n_j denotes the IMFs number of the j^{th} ensemble. By calculating the ensemble means of corresponding IMFs of the decompositions, the final IMF obtained by the EEMD algorithm is given by:

$$\hat{c}_i(t) = \frac{\sum_{j=1}^{NE} c_{i,j}(t)}{NE}, \ i = 1, 2, \ldots, \hat{n} \tag{4}$$

where $\hat{n}$ = min (n_1,n_2,. . .n_{NE}). For the sake of convenience, the algorithm of EEMD is summarized as follows:

1. Determine an optimal noise amplitude and a proper ensemble number (Please observe Section 2.3).
2. Perform the jth ensemble on the noise-added signal xj(t) by j = 1.
   - 2a. Generate a randomly zero mean unit variance white noise signal with the obtained noise amplitude and add it to the original signal.
   - 2b. Decompose the noise-added signal into n modes (ci,j) using the EMD algorithm.
   - 2c. If j < NE, then return to step 2a with j = j + 1.
   - 2d. Repeat steps 2a-2c again with a new randomly white noise signal.
3. Calculate the ensemble mean of the NE trails for each IMF based on Eq. (4).
4. Apply the mean ĉi as the final IMF obtained by the EEMD method.

2.3. Parameter selection

The amplitude of the added white noise and the ensemble number are crucial parameters in the EEMD algorithm that need to be prescribed. In general, there are no specific formulations to determine the EEMD parameters, particularly the noise amplitude. In most cases, these values are obtained from the trial and error or empirical equations [28]. For instance, Wu and Huang [11] provided a relationship among the ensemble number, the noise amplitude, and the standard deviation of error. They recommended that the amplitude of the added white noise is approximately 0.2 of a standard deviation of the original signal and the value of ensemble number is a few hundred. However, this approach is not always useful for signal processing in various applications, because the noise amplitude has a considerable importance in the performance of the EEMD method. Selection of a very low-value noise amplitude will not introduce adequate changes in the extremes of the decomposed signal and a very high quantity will result in redundant IMFs. In order to have an accurate choice of A_n, one can introduce relative root-mean-square of error (R_{RMSE}) method [28] as follows:

$$R_{RMSE} = \sqrt{\frac{\sum_{k=1}^{nt} (x(k) - c_{max}(k))^2}{\sum_{k=1}^{nt} \left(x(k) - \bar{x}\right)^2}} \tag{5}$$

where c_{max} is an IMF that has the highest correlation with the original signal; nt denotes the number of time samples, and $\bar{x}$ represents the mean of the original signal. If the value of R_{RMSE} to be small, the selected IMF is close to the original signal with the availability of white noise. It implies that c_{max} not only includes the main component of the original signal, but also involves the noise and/or the other irrelevant signal components. Accordingly, the difference between the original signal and the selected IMF becomes small, which indicates an inappropriate decomposition process. On the contrary, a high value of R_{RMSE} means that the signal is separated from the noise and the other irrelevant signal components; hence, the selected IMF consists of the main signal component. It is worth remarking that the amplitude of the added white noise is related to the original signal and can be expressed as follows:

$$A_n = L_n \sigma_0 \tag{6}$$

where σ_0 is the standard deviation of the original signal and L_n denotes the noise level of the added white noise. Therefore, the selection of A_n is equivalent to choosing L_n. Once the noise amplitude has been determined, one needs to obtain a proper ensemble number; however, this procedure may have two significant limitations. First, the selection of a large ensemble quantity will lead to a high computation cost. Second, a small number of N_E will not enable the EEMD method to cancel out the noise remaining in each IMF [28]. In this regard, a reliable approach to determining a suitable ensemble number is the signal-to-noise ratio (SNR). This process is based on fixing the optimal noise amplitude and increasing the ensemble number until the change in the value of SNR relatively becomes small.

3. Time series analysis by ARARX model

A time series is a sequence of observations measured sequentially in a specific time interval. It appears as stationary or non-stationary, seasonal or non-seasonal, deterministic or random, and linear or non-linear data. On the other hand, time series analysis is a statistical tool that aims at analyzing time series data by fitting a mathematical model for various tasks such as time series modeling, feature extraction, and forecasting [25]. A time series representation is a stochastic model building of time series that depends on the nature of data. Assuming that vibration time-domain signals (i.e. accelerations or IMFs) are stationary and linear, one can build diverse polynomial time-invariant linear models such as AR, ARX, ARMA, ARMAX, and ARARX [25,29]. Generally, these representations consist of three main parts: (i) *eXogenous* (X) or input term related to the excitation forces subjected to the structure, (ii) *autoregressive* (AR) or output term regarding the structural responses, and (iii) *moving average* (MA) or error term [29].

In the case of using the ambient vibrations, when the input data is unmeasurable and unknown, an efficient way for the response modeling is to apply time series models that incorporate a polynomial equation into the error term. This is because of the fact that changes in the amplitude of ambient excitations will lead to alterations in the coefficients of the MA term [22]. Among the above-mentioned time-invariant linear models, one can utilize the ARMA and ARARX representations for modeling the vibration time-domain signals under the ambient excitations. Note that although the ARMAX model contains the error term, it is not usually used in the modeling process resulting from the unavailability of input data.

On the other hand, the selection of ARMA or ARARX depends on the nature of data. In some circumstances, a time series signal may only conform to an AR process, which makes possible to choose the ARARX model rather than ARMA [29]. One efficient way to find the nature of time series data is to apply Box-Jenkins methodology by checking the correlation of data using autocorrelation function (ACF) and partial autocorrelation function (PACF) [25]. According to this methodology, if ACF tails off as exponentially decay or damped wave sine and PACF cuts off after a certain lag, it implies that time series data is compatible with the AR process. In contrast, if ACF cuts off after a certain lag and PACF decays gradually as exponential or damped sine waveforms, time series data conforms to the MA process. Eventually, if both ACF and PACF decay gradually, it is preferable to consider the ARMA model. Given a stationary and linear vibration response $y(t)$, the AR representation is expressed as:

$$y(t) = \sum_{\mathrm{i}=1}^{p} \theta_{\mathrm{i}} y(t-\mathrm{i}) + e(t) \tag{7}$$

where $\Theta=[\theta_1,\theta_2,\ldots,\theta_p]$ and p represent the AR model coefficients and order, respectively. Moreover, $e(t)$ denotes the residual sequence at time t, which corresponds to the difference between the measured vibration signal and the predicted one obtained from the model. The general idea behind the establishment of an ARARX model is to use the residuals of the AR model as the input data in the ARX representation as follows:

$$y(t) = \sum_{\mathrm{j}=1}^{q} \varphi_{\mathrm{j}} y(t-\mathrm{j}) + \sum_{\mathrm{k}=1}^{r} \psi_{\mathrm{k}} e(t-\mathrm{k}) + \varepsilon(t) \tag{8}$$

where q and r are the orders of ARX model associated with the output and input terms, for which $\mathbf{\Phi}=[\varphi_1,\varphi_2,\ldots,\varphi_q]$ and $\mathbf{\Psi}=[\psi_1,\psi_2,\ldots,\psi_r]$ are their coefficients, respectively. In Eq. (8), $\varepsilon(t)$ denotes the residual of the ARX model at time t. The significant topic in time series modeling is to determine sufficient orders so that enable the time series model to produce uncorrelated (independent) residuals [25]. If the model orders to be inadequate, it is essential to improve them for fitting an accurate time series model and capturing the entire information about the structural dynamics [30]. Due to the importance of order determination in time series modeling, an iterative method proposed by the current authors [24] is utilized to choose the sufficient orders for the AR and ARX terms of the ARARX model.

4. A new feature extraction method by EEMD-ARARX algorithm

The proposed feature extraction method is a two-stage hybrid algorithm as the combination of the EEMD method and ARARX model (EEMD-ARARX). Although some researchers exploited the EMD-AR algorithm [31,32], it may fail in extracting the reliable and informative DSFs for some reasons. First, the mode mixing problem mainly occurs in the signal decomposition procedure by using the EMD technique. Second, the AR model is not usually suitable for modeling the vibration time-domain responses acquired from the ambient excitations. The main objective of the proposed EEMD-ARARX algorithm is to extract the significant DSFs from non-stationary and/or stationary signals under unmeasurable ambient vibration. In the first stage, an IMF with the highest energy level among all modes extracted from the EEMD method is obtained as the main IMF to use in the ARARX modeling. The primary advantage of this mode is that it strongly depends on the damage. The total energy of all IMFs (E_T) is given by:

$$E_T = \sum_{\mathrm{i}=1}^{n} E_{\hat{c}_{\mathrm{i}}(t)} \tag{9}$$

where $E_{\widehat{c_{\mathrm{i}}(t)}}$ denotes the amount of energy contained in the i$^{\text{th}}$ IMF, which can be expressed as:

$$E_{\hat{c}_{\mathrm{i}}(t)} = \sum_{\mathrm{k}=1}^{nt} |\hat{c}_{\mathrm{i}}(k)|^2 \tag{10}$$

Due to being stationary, the selected IMF is highly proper to utilize in the time-invariant linear representations for time series modeling. Accordingly, the second stage is concerned with modeling the main IMF through an ARARX representation. This process consists of: (i) the determination of the AR and ARX orders in the normal (healthy or known) condition, (ii) estimation of the model coefficients, and (iii) extraction of the model residuals in both healthy and damaged (abnormal or current) states. Fig. 1 shows the flowchart of the proposed EEMD-ARARX algorithm. In this figure, $\mathbf{z}_{\mathrm{AR}}$ and $\mathbf{z}_{\mathrm{ARX}}$ denote the residual vectors of the AR and ARX models, respectively.

In SHM community, the process of feature extraction by time series modeling consists of coefficient-based and residual-based methods [24]. For the sake of convenience and clarification, these algorithms are developed to describe the extraction of DSFs based on the EEMD-ARARX algorithm. In the first method, the AR coefficients of the ARX model are representative of damage features, for which the model orders (p, q, and r) are initially determined in the normal condition. Suppose that $x_u(t)$ and $x_d(t)$ are the vibration time-domain signals in the undamaged and damaged conditions. Applying the EEMD method, the main IMFs of both signals are extracted and designated by $c_{mu}(t)$ and $c_{md}(t)$, respectively. Having the orders of AR and ARX representations into consideration, the expressions needed to obtain the model coefficients in the normal condition are written in the following forms:

$$c_{mu}(t) = \sum_{\mathrm{i}=1}^{p} \theta_{u_{\mathrm{i}}} c_{mu}(t-\mathrm{i}) + e_u(t) \tag{11}$$

$$c_{mu}(t) = \sum_{\mathrm{j}=1}^{q} \varphi_{u_{\mathrm{j}}} c_{mu}(t-\mathrm{j}) + \sum_{\mathrm{k}=1}^{r} \psi_{u_{\mathrm{k}}} e_u(t-\mathrm{k}) + \varepsilon_u(t) \tag{12}$$

The same formulations can be expressed for the current or damaged state as:

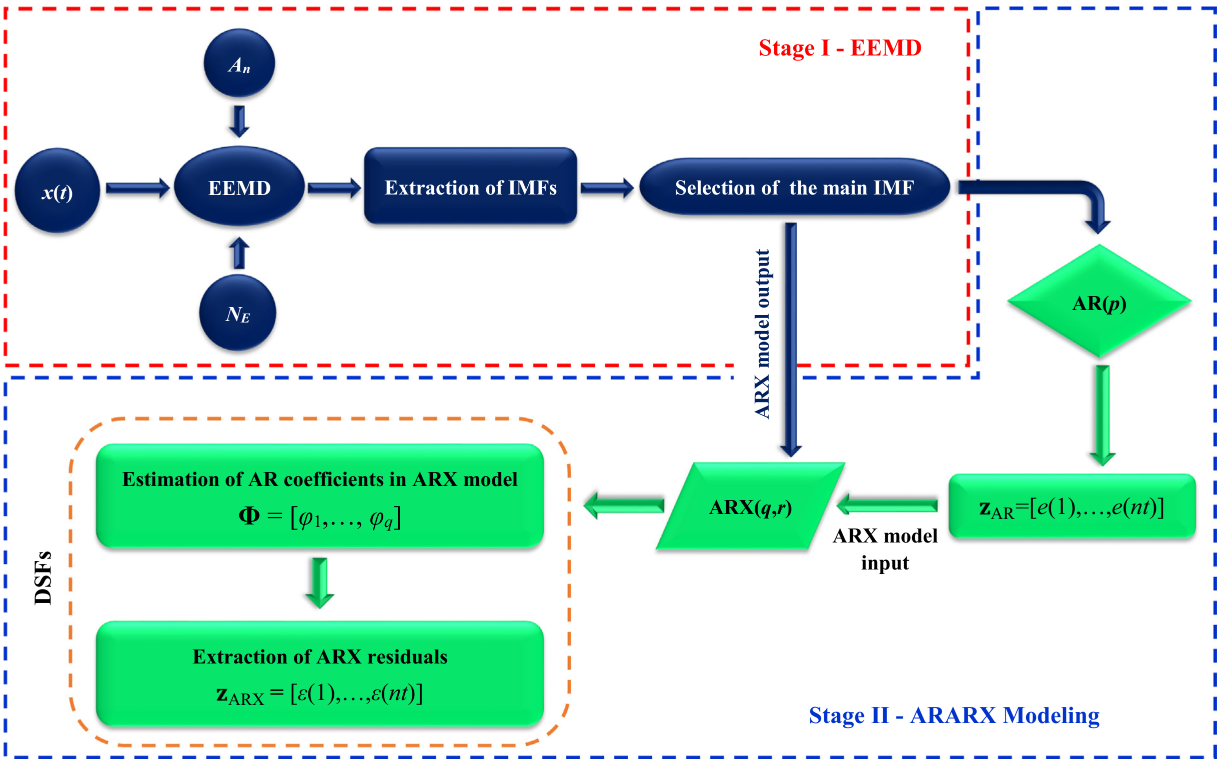

Fig. 1. The flowchart of the proposed EEMD-ARARX algorithm.

$$c_{md}(t) = \sum_{i=1}^{p} \theta_{d_i} c_{md}(t-i) + e_d(t) \tag{13}$$

$$c_{md}(t) = \sum_{j=1}^{q} \varphi_{d_j} c_{md}(t-j) + \sum_{k=1}^{r} \psi_{d_k} e_d(t-k) + \varepsilon_d(t) \tag{14}$$

Based on these formulations, the AR coefficients of the ARX representation in both normal and damaged states, $\mathbf{\Phi}_u = [\varphi_{u1}\ldots\varphi_{uq}]$ and $\mathbf{\Phi}_d = [\varphi_{d1}\ldots\varphi_{dq}]$, are selected as the DSFs. The residual-based feature extraction method relies upon using the model orders and coefficients in the normal condition for predicting the responses of the damaged state. The fact beyond this algorithm is that the model (i.e. its orders and coefficients) used in the undamaged state will no longer correctly predict the responses of the damaged structure. Thus, the model residuals regarding the damaged state will increase. Considering the ARARX model orders and coefficients (i.e. Θ_u, $\mathbf{\Phi}_u$, and $\mathbf{\Psi}_u$) obtained from the normal condition, the ARX residuals associated with the undamaged and damaged states are extracted as the DSFs in the following forms:

$$\varepsilon_u(t) = c_{mu}(t) - \left[\sum_{j=1}^{q} \varphi_{u_j} c_{mu}(t-j) + \sum_{k=1}^{r} \psi_{u_k} e_u(t-k)\right] \tag{15}$$

$$\varepsilon_u(t) = c_{md}(t) - \left[\sum_{j=1}^{q} \varphi_{u_j} c_{md}(t-j) + \sum_{k=1}^{r} \psi_{u_k} e_d(t-k)\right] \tag{16}$$

5. Feature classification methods

5.1. DTW

The DTW is a distance method that computes the dissimilarity between two time-domain sequences by finding an optimal path between them [33]. More precisely, it measures the dissimilarity by aligning the two sequences of possibly different lengths and computing a distance function using dynamic programming. Actually, the sequences are warped in a non-linear manner to calculate the dissimilarity, regardless of the non-linear variations [34,35]. The primary aim of using the DTW method is to locate damage using the AR coefficients of the ARX model as the DSFs. For this purpose, the DTW calculates a distance matrix as the dissimilarity of all samples between $\mathbf{\Phi}_u$ and $\mathbf{\Phi}_d$ as follows:

$$\boldsymbol{D} = \begin{bmatrix} d_{11} & & \cdots & & d_{q1} \\ & \ddots & & \cdots & \\ \vdots & & d_{ij} & & \vdots \\ & \cdots & & \ddots & \\ d_{1q} & & \cdots & & d_{qq} \end{bmatrix} \tag{17}$$

where d_{ij} represents the dissimilarity between ith sample of $\mathbf{\Phi}_u$ and jth sample of $\mathbf{\Phi}_d$. Typically, the Euclidean distance function is applied to calculate point-to-point dissimilarity in the following form:

$$d_{ij} = \left(\varphi_{u_i} - \varphi_{d_j}\right)^2, \qquad i,j = 1,2,\ldots,q \tag{18}$$

Once the distance matrix has been established, the optimal path warp is computed by using the minimum cumulative distance between the sequences. The best match between two sequences is one that has the lowest distance path warp after aligning one sequence to the other. The dissimilarity between $\mathbf{\Phi}_u$ and $\mathbf{\Phi}_d$ based on the DTW method corresponds to the path with minimal warping cost as follows:

$$DTW(\mathbf{\Phi}_u, \mathbf{\Phi}_d) = \sqrt{\Gamma(i,j)} \tag{19}$$

where

$$\Gamma(\mathrm{i,j}) = \left(\varphi_{u_i} - \varphi_{d_j}\right)^2 + \min\begin{Bmatrix} \Gamma(\mathrm{i-1,j-1}) \\ \Gamma(\mathrm{i-1,j}) \\ \Gamma(\mathrm{i,j-1}) \end{Bmatrix} \tag{20}$$

For the process of damage localization, one can obtain a DTW distance value at each sensor location. Assuming that *ns* sensors are installed on the structure of interest, the damage localization vector is given by **DLV**=[$DTW_1 \ldots DTW_{ns}$]. The location of damage is situated near a sensor that has a larger DTW quantity in comparison with the other sensors. One robust way to make sure of locating damage is to define a threshold limit. A common approach is to use a statistical confidence interval of the **DLV** amounts [36]. On this basis, the threshold is expressed as the upper bound of a one-sided confidence interval in the following form:

$$\tau = \mu_{DLV} + \left(\frac{\sigma_{DLV}}{\sqrt{ns}}\right) f_{(1-\alpha)} \tag{21}$$

where μ_{DLV} and σ_{DLV} are the mean and standard deviation of the **DLV** amounts, respectively. Furthermore, $f_{(1-\alpha)}$ is the critical value for the distribution with *ns*-1 degree of freedom in α significant level. Applying 5% significant level, the threshold is based on the upper bound 95% confidence interval. For the problem of damage localization, the sensor location regarding the DTW dissimilarity value more than the threshold limit is identified as the location of damage.

5.2. CDTW

Although the DTW method measures the dissimilarity between two time-domain sequences appropriately, it may suffer a major drawback regarding the distance computation of high-dimensional time series data. The ARX residual vector of the ARARX model at each sensor location has the same number of samples as the original signal, which is a relatively large and high-dimensional time series set for feature classification. Therefore, the direct use of the DTW method may not be suitable for early damage detection due to making a complicated and time-consuming process. For this reason, the CDTW method is presented here to deal with the DTW shortcomings. This method relies on the segmentation of multivariate high-dimensional time series data using principal component analysis (PCA) [37].

On the other hand, the problem of early damage detection by using the residuals of time series models lies in the fact that the occurrence of damage changes the correlation of residual sequences. As stated earlier, the model residuals gained by the normal condition of the structure should be uncorrelated. On this basis, any change in the residual correlation is indicative of the damage occurrence [24]. Therefore, in addition to dealing with the significant issue of using the high-dimensional features, the CDTW method is efficiently suitable for the problem of early damage detection.

The main aim of data segmentation in the CDTW is to find homogenous partitions by defining a cost function. Suppose that **Z** is an *nt*-element *ns*-variable multivariate time series, which can be expressed as:

$$\begin{aligned} \boldsymbol{Z} &= [\boldsymbol{z}_1, \boldsymbol{z}_2, \ldots \boldsymbol{z}_\mathrm{i}, \ldots, \boldsymbol{z}_\mathrm{ns}], \\ \boldsymbol{z}_\mathrm{i} &= [\mathrm{z_i}(1), \mathrm{z_i}(2), \ldots, \mathrm{z_i}(\mathrm{j}), \ldots, \mathrm{z_i}(nt)]^\mathrm{T} \end{aligned} \tag{22}$$

where $\mathbf{z}_i$ is the ith variable and z_i(j) denotes the jth element of $\mathbf{z}_i$. Based on this notation, a multivariate time series data set can be represented by a matrix, in which each column (variable) corresponds to a vector ($\mathbf{z}_i$) and each row denotes a sample of the multivariate time series, z_i(j), as follows:

$$\begin{bmatrix} \boldsymbol{Z}(1) \\ \boldsymbol{Z}(2) \\ \vdots \\ \boldsymbol{Z}(nt) \end{bmatrix} = \begin{bmatrix} z_1(1) & z_2(1) & \cdots & z_{ns}(1) \\ z_1(2) & z_2(2) & \cdots & z_{ns}(2) \\ \vdots & \vdots & \vdots & \vdots \\ z_1(nt) & z_2(nt) & \cdots & z_{ns}(nt) \end{bmatrix} \tag{23}$$

The ith segment of **Z** is a set of consecutive time samples, $\mathbf{S}_i(a,b)$=[$\mathbf{Z}(a)$;$\mathbf{Z}(a+1)$;...;$\mathbf{Z}(b)$], where *a* and *b* are the first and last samples. The ν-segmentation of the multivariate time series is a partition of **Z** to ν non-overlapping segments as $\mathbf{S_Z}$=[$\mathbf{S}_1(1,a)$;$\mathbf{S}_2(a+1,b)$;...;$\mathbf{S}_\nu(k, nt)$]. Indeed, a ν-segmentation splits **Z** to ν disjoint time intervals, where $1 \le a$ and $k \le nt$. The cost function for segmentation can be any arbitrary equation that projects the multivariate time series data set to the space of the non-negative real numbers [37]. It is usually based on the differences between the segment values and its approximation by a simple function (g) as follows:

$$Cost(\boldsymbol{S}_\mathrm{i}(a,b)) = \frac{1}{b-a+1}\sum_{\mathrm{j}=a}^{b} \mathrm{d}(\boldsymbol{Z}(\mathrm{j}), g(\boldsymbol{Z}(\mathrm{j}))) \tag{24}$$

In this study, Hotelling's T^2 statistic and Q-reconstruction error (QRE) are used to define their cost functions and segment the multivariate data sets as the measure of the homogeneity of segments. The QRE employs the direct change in the correlation among variables, whereas the Hotelling's T^2 statistic is a statistical measure of the multivariate distance of each sample from the center of the data set. For the jth sample, the QRE and Hotelling's T^2 statistic are expressed as:

$$\mathrm{Q}(\mathrm{j}) = \boldsymbol{Z}(\mathrm{j})\left(\boldsymbol{I} - \boldsymbol{U}_{pc}\boldsymbol{U}_{pc}^\mathrm{T}\right)\boldsymbol{Z}(\mathrm{j})^\mathrm{T} \tag{25}$$

$$T^2(\mathrm{j}) = \boldsymbol{L}_{pc}(\mathrm{j})\boldsymbol{L}_{pc}(\mathrm{j})^\mathrm{T} \tag{26}$$

where **I** is the identity matrix; $\mathbf{U}_{pc}$ represents the matrix of principal components gained by the PCA and $\mathbf{L}_{pc}$(j) is the lower ν-dimensional representation of **Z**(j). Based on Eq. (24), the cost functions of QRE and Hotelling's T^2 statistic are given by:

$$Cost_Q(\boldsymbol{S}_\mathrm{i}(a,b)) = \frac{1}{b-a+1}\sum_{\mathrm{j}=a}^{b} \mathrm{Q}(\mathrm{j}) \tag{27}$$

$$Cost_{T^2}(\boldsymbol{S}_\mathrm{i}(a,b)) = \frac{1}{b-a+1}\sum_{\mathrm{j}=a}^{b} T^2(\mathrm{j}) \tag{28}$$

Before utilizing PCA-based segmentation techniques, it is essential to determine the adequate numbers of principal components (n_{PC}) and segments (ν). Average eigenvalue criterion (AEC) or Kaiser's criterion is one of the methods for determining n_{PC}, which adopts the only significant components with eigenvalue larger than the average eigenvalue. In order to obtain ν, an efficient and simple approach is to use relative reduction error of the cost function between two consecutive segments as presented in the following equation [37]:

$$\rho_r = \frac{Cost\left(\boldsymbol{S}^{\nu-1}\right) - Cost\left(\boldsymbol{S}^{\nu}\right)}{Cost\left(\boldsymbol{S}^{\nu-1}\right)} \tag{29}$$

In this equation, $Cost(\mathbf{S}^{\nu-1})$ and $Cost(\mathbf{S}^{\nu})$ are the cost functions of QRE or Hotelling's T^2 statistic for ν-1 and ν segments. The appropriate number of segments is one that has the smallest ρ_r.

Now, suppose that $\mathbf{Z_u}$ and $\mathbf{Z_d}$ are the ARX residuals of the ARARX model in the normal and damaged conditions. Both of them are matrices with *nt* samples (rows) and *ns* variables (columns), which make randomly high-dimensional multivariate data sets. Initially, the PCA-based segmentation techniques based on the QRE and

Hotelling's T^2 cost functions are applied to determine the segments of these multivariate datasets in the normal and damaged conditions ($\mathbf{S_u}$ and $\mathbf{S_d}$). The early damage detection is based on the calculation of CDTW dissimilarity quantity using PCA similarity factor as follows [38]:

$$DS(\mathbf{Z_u}, \mathbf{Z_d}) = \frac{trace\left(\mathbf{S}_u^T\mathbf{S}_d \cdot \mathbf{S}_d^T\mathbf{S}_u\right)}{n_{PC}} \tag{30}$$

where *trace* denotes the sum of the diagonal elements of $\left(\mathbf{S}_u^T\mathbf{S}_d \cdot \mathbf{S}_d^T\mathbf{S}_u\right)$. Based on Eq. (30), the *DS* quantity close to zero is representative of the normal condition and any deviation from this amount implies the occurrence of damage. Furthermore, the largest *DS* value represents the highest level of damage severity.

6. Application

To validate the accuracy and performance of the proposed methods, a series of experimental data sets of the well-known IASC-ASCE benchmark model (Phase II) are applied. This is a four-story steel structure, as shown in Fig. 2(a), constructed from 2-bay-by-2-bay steel frame in scale-model with 2.5 × 2.5 m in plan and 3.6 m in tall [39]. The members were hot-rolled grade 300 W steel with the nominal yield stress 300 MPa. The columns and floor beams were constructed by B100 × 9 and S75 × 11 sections, respectively. In each bay, the bracing system consisted of two 12.7 mm diameter threaded steel rods placed in parallel along the diagonal.

Different structural changes were considered to simulate damage cases with different severity levels. The damage patterns included removing the bracing systems from the east side of the structure and loosening the bolts at the beam-column connections on the east-north side. In this study, the first damage pattern is used to assess the capability of the proposed methods. Table 1 represents the healthy and damaged conditions of this pattern.

A relatively dense sensor network with 15 accelerometers was mounted on the structure to measure acceleration time-domain responses caused by the ambient excitations such as wind, pedestrians, and traffic. As Fig. 2(b) appears, two accelerometers were placed along the east and west frames on each floor as well as the base of the structure to measure the motion in the north-south direction (along the strong axis). Additionally, an accelerometer was installed on each floor and the base near the center column of the frame to measure the east-west accelerations of the structure (along the weak axis). Applying a sampling frequency of 200 Hz, 60,000 samples of vibration signals were measured during a time window of 300 s. It is important to point out that the acceleration time-domain responses acquired from the sensors 1–3 mounted on the base are not incorporated into the feature extraction and classification steps owing to the lack of having relevant information about the dynamic behavior of the structure. For example, Figs. 3–5 demonstrate the vibration signals of the sensors 4–15 associated with the cases 1, 2, and 5, respectively. In addition, some statistical analyses are performed on the measured acceleration responses of all cases to show their statistical properties as illustrated in Figs. 6 and 7. These can be applied to assess the uncertainty in measurement. It is worth remarking that if an uncertainty is based on a statistical analysis, it is treated as a Type A uncertainty [40,41]. Furthermore, it needs to mention that due to using the unmeasurable and unknown ambient vibration for the excitation of the structure, the problem is most likely a Type A uncertainty [41].

6.1. Initial data analysis

Prior to implementing the step of feature extraction, it is preferable to analyze the vibration time-domain responses. To perform this task, each vibration signal is initially normalized by the *z*-score standardization procedure through subtracting all samples from the mean of the signal and diving its standard deviation. Subsequently, the stationarity of vibration responses is assessed by using Kwiatkowski-Phillips-Schmidt-Shin (KPSS) hypothesis test [42]. It assesses the null hypothesis that a univariate time series is trend stationary against the alternative hypothesis that it is a

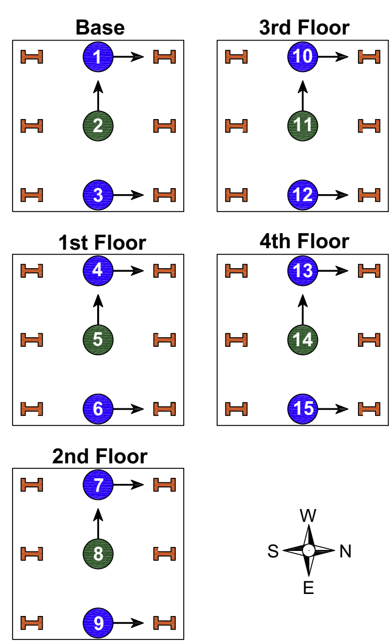

(a) (b)

Fig. 2. (a) The view of the IASC-ASCE benchmark structure, (b) the sensor locations.

Table 1
Damage scenarios of the second phase of the IASC-ASCE structure.

Case no.	Condition	Description
1	Healthy	Fully braced configuration
2	Damaged	Removing the braces of all floors from the east side
3	Damaged	Removing the braces of all floors from one bay on the southeast corner
4	Damaged	Removing the braces of the first and fourth floors from one bay on the southeast corner
5	Damaged	Removing the braces of the first floor from one bay on the southeast corner

non-stationary unit root process. The KPSS test gives important outputs such as a test statistic, a critical value (c-value), and a probability value (p-value) that can be utilized to analyze time series data. By using a significant limit (α), it is possible to make a decision about the null or alternative hypotheses. If the test statistic is less than the c-value or the p-value to be more than the significant limit, these imply that the time series data is stationary.

As a sample, Fig. 8 illustrates the KPSS test statistics by considering the 95% confidence interval under 5% significant level at all sensors for the cases 1–4. In this figure, the red lines depict the c-value of the KPSS test, which corresponds to 0.1460. It is clear in Fig. 8 that some vibration signals have non-stationary behaviors and the other ones are stationary. Such observations clearly demonstrate the effect of unknown ambient excitations on the responses of the structure. Under such circumstances that the nature of vibration responses is variable and unpredictable, one of the most suitable ways for the feature extraction is to use a combination of a signal decomposition method and a time series model such as the proposed EEMD-ARARX algorithm. Although this method is usually proper to decompose the non-stationary signals

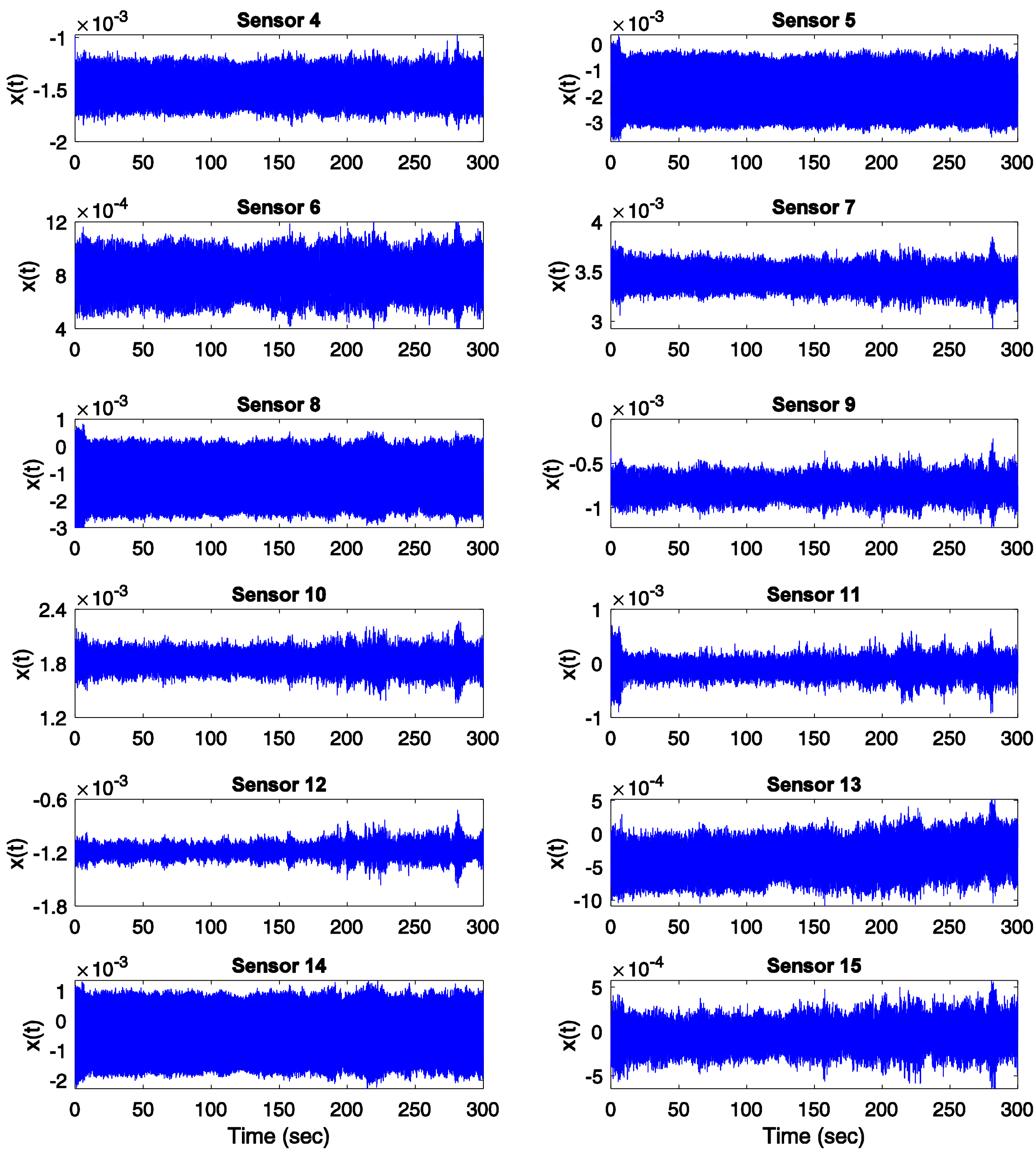

Fig. 3. The vibration signals of the sensors 4–15 of the IASC-ASCE structure in the case 1.

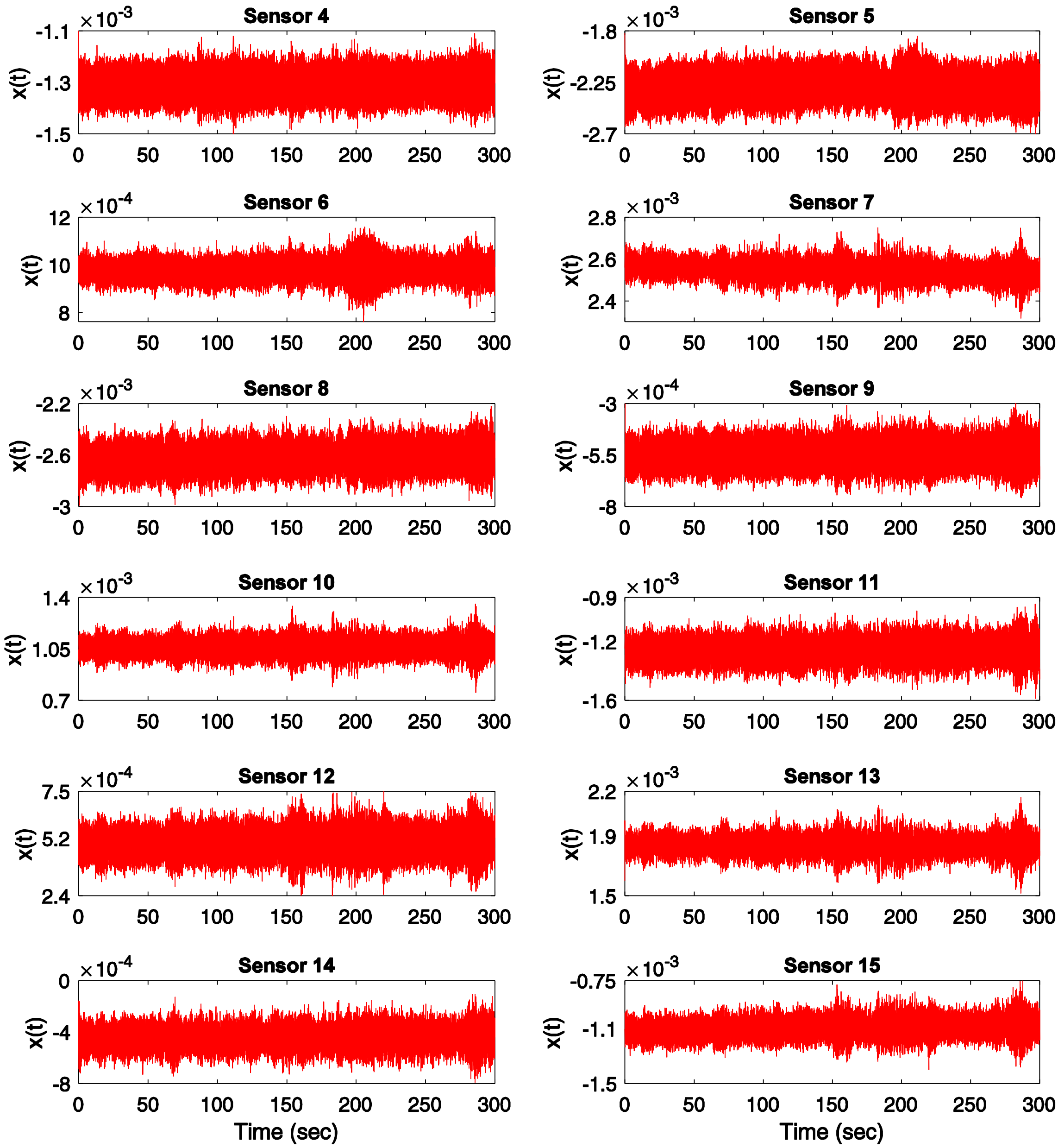

Fig. 4. The vibration signals of the sensors 4–15 of the IASC-ASCE structure in the case 2 (the highest level of damage).

into several stationary IMFs, there is no limitation to use it for the stationary data.

6.2. Parameter selection for EEMD

In the first stage of the proposed feature extraction method based on the EEMD-ARARX algorithm, one should choose an optimal noise amplitude and an appropriate ensemble number for the extraction of true IMFs. At first, a wide range of noise levels (L_n) is chosen to use in the EEMD method and then calculate their R_{RMSE} values based on Eq. (5). For this process, the initial ensemble number is set as a small value, $NE = 10$, and relatively large and small amounts are chosen as the initial and last noise levels, $(L_n)_1 = 2.5$ and $(L_n)_{\text{Last}} = 0.001$. According to these values, three different ranges of the noise levels are defined to obtain an optimal L_n that makes the largest R_{RMSE} quantity. In the first range, the noise level decreases from 2.5 to 0.1 in the step of 0.1 ($2.5 \geq L_n \geq 0.1$). For the second range, this process repeats between 0.09 and 0.01 ($0.1 > L_n \geq 0.01$) in the step of 0.001. Finally, in the third range of the noise level, it begins with 0.009 and ends with the last noise level ($0.01 > L_n \geq 0.001$), in which the decreasing step becomes 0.001. Fig. 9 indicates the selection of optimal noise level at some sensors of the cases 1–4.

Once the optimal noise amplitudes based on Eq. (6) have been determined, the process of selecting appropriate ensemble numbers is carried out by fixing the optimal A_n and increasing N_E until the alteration in the SNR values relatively becomes small. This procedure is shown in Fig. 10 for some sensors in the cases 1–4. The initial ensemble number is set as 10 and the other numbers are 30, 50, 100, 120, 150, 180, 200, 250, and 300. Note that the same process with Fig. 10 is accomplished to attain the proper ensemble numbers for the other sensors in all cases.

From Figs. 9 and 10, it can be observed that the amounts of A_n and N_E in the different structural conditions (the cases 1–4) and

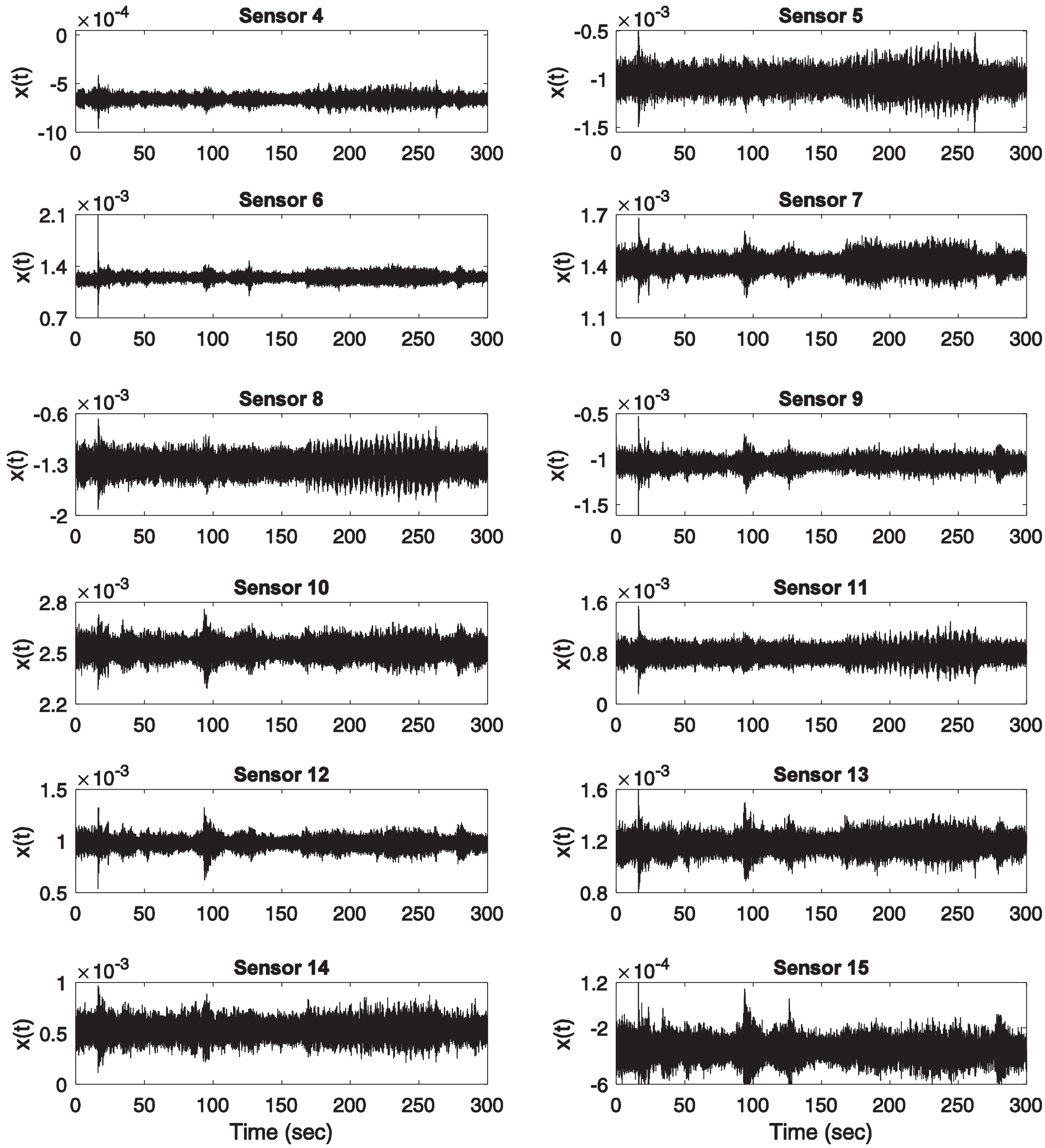

Fig. 5. The vibration signals of the sensors 4–15 of the IASC-ASCE structure in the case 5 (the lowest level of damage).

sensors approximately vary in the same levels so that the noise levels and the ensemble numbers are in the ranges of 1.1–1.5 and 100–150, respectively. These mean that the unknown and unpredictable ambient excitations, which may lead to stationary or non-stationary vibration signals, do not significantly affect the process of parameter selection.

6.3. IMF extraction

Applying the obtained noise amplitudes and ensemble numbers to the EEMD algorithm, the true IMFs of each vibration signal are extracted. At each sensor, the main IMF with the highest energy level is selected among all extracted modes in both healthy (c_{mu}) and damaged (c_{md}) states. For instance, the energy levels of all IMFs in the cases 1–4 at the sensor 15 are illustrated in Fig. 11.

From Fig. 11, one can observe that the most relevant IMFs to the original vibration signal are available in the first few modes, which include larger energy levels and frequency contents in comparison with the other modes. In other words, these IMFs are the main components of the vibration signals, which have the major dynamic information. Among them, the main IMF with the highest energy level is selected as the candidate of all extracted IMFs to utilize in the ARARX modeling and feature extraction.

As another note, the main advantage of the signal decomposition methods such as EEMD is to convert a non-stationary vibration signal into several stationary components or modes. Due to being stationary, one can simply apply the time-invariant linear representations such as the ARARX model to extract the DSFs. In this regard, Fig. 12 indicates the non-stationary vibration signals (i.e. after the z-score standardization) at the sensor 15 in the cases 1 and 2 as well as their stationary main IMFs. To ensure the stationarity of extracted IMFs, Fig. 13 shows the results of the KPSS hypothesis test at all sensors in the cases 1–4. Using the 5% significant limit and 95% confidence

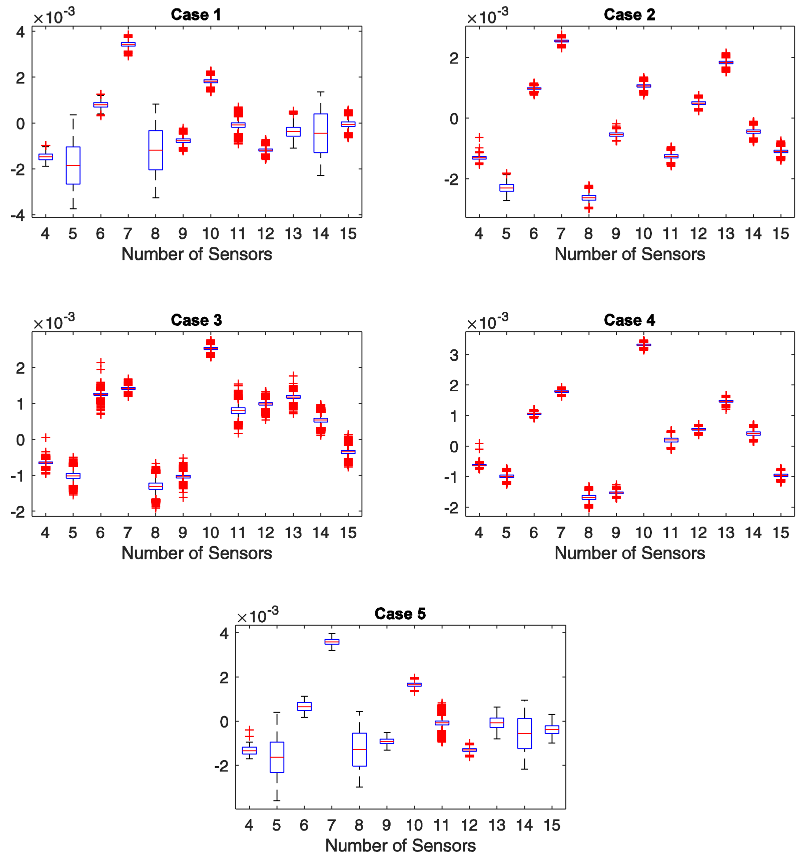

Fig. 6. Box plots of the vibration signals of the IASC-ASCE structure in all cases.

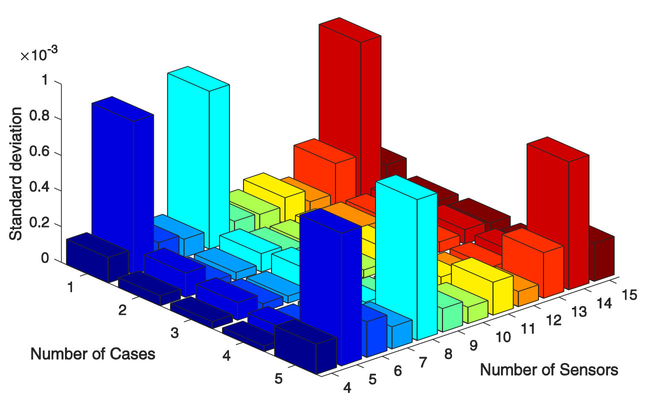

Fig. 7. Standard deviations of the vibration signals of the IASC-ASCE structure in all cases.

interval, the *c*-value of the test corresponds to 0.1460. Accordingly, it is discerned that all test statistics are less than the *c*-value in the sense that the main IMFs is compatible with the stationary process.

6.4. ARARX modeling

In the second stage of the proposed hybrid algorithm, the ARARX model is fitted to the main IMF at each sensor. Before this process, it is necessary to clarify the reason for choosing the ARARX representation among all time-invariant linear models. As already stated, the ARMA and ARARX models are suitable for situations that the input data caused by the ambient excitations are unknown and unmeasurable.

From a statistical viewpoint, the difference between these models is that the ARARX model is entirely compatible with the AR process, whereas the ARMA representation conforms to both AR and MA processes. Using the Box-Jenkins methodology for the model identification, Fig. 14 indicates the ACF and PACF of the main IMFs at the sensor 15 of the cases 1 and 2. It is obvious that the ACF patterns do not tend to be zero and roughly behave as a sine wave, whereas the PACF patterns approximately become zero after 25th lag. Such observations prove that the main IMFs are compatible with the AR process. Therefore, it is an accurate choice to use ARARX rather than ARMA for time series modeling.

In the following, the orders of AR and ARX terms of the ARARX model are determined by the iterative order determination method presented in [24]. This method is based on the residual analysis by Ljung-Box hypothesis test for checking the uncorrelatedness of the model residuals. The main premise of the iterative method lies in the fact that a sufficient order is one that enables the time series model to produce the uncorrelated residuals. Using 5% significant limit, if the *p*-value of the test to be more than 0.05, one can argue that the model residuals are uncorrelated. On this basis, the number of iterations that satisfies this criterion is chosen as an adequate order. Table 2 presents the amounts of p, q, and r along with the *p*-values of the Ljung-Box hypothesis test in the healthy state. It is important to note that the equal orders are considered for the ARX model ($q = r$).

The amounts in Table 2 show that the obtained orders enable the AR and ARX models to make uncorrelated residuals since the *p*-values at all sensors are greater than 0.05. As another conclusion, one can observe that the sum of q and r is smaller than p at each sensor. This is Ljung's suggestion for avoiding the overfitting prob-

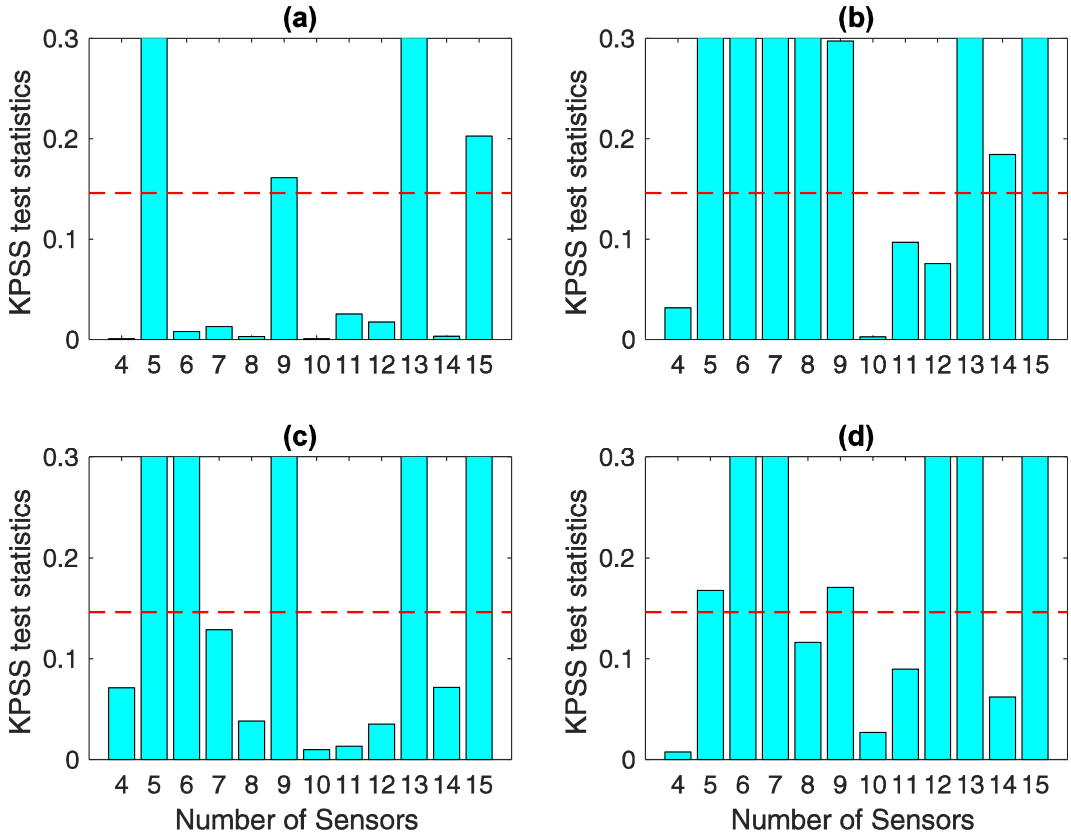

Fig. 8. Stationarity assessment of the vibration signals by the KPSS hypothesis test: (a) Case 1, (b) Case 2, (c) Case 3. (d) Case 4.

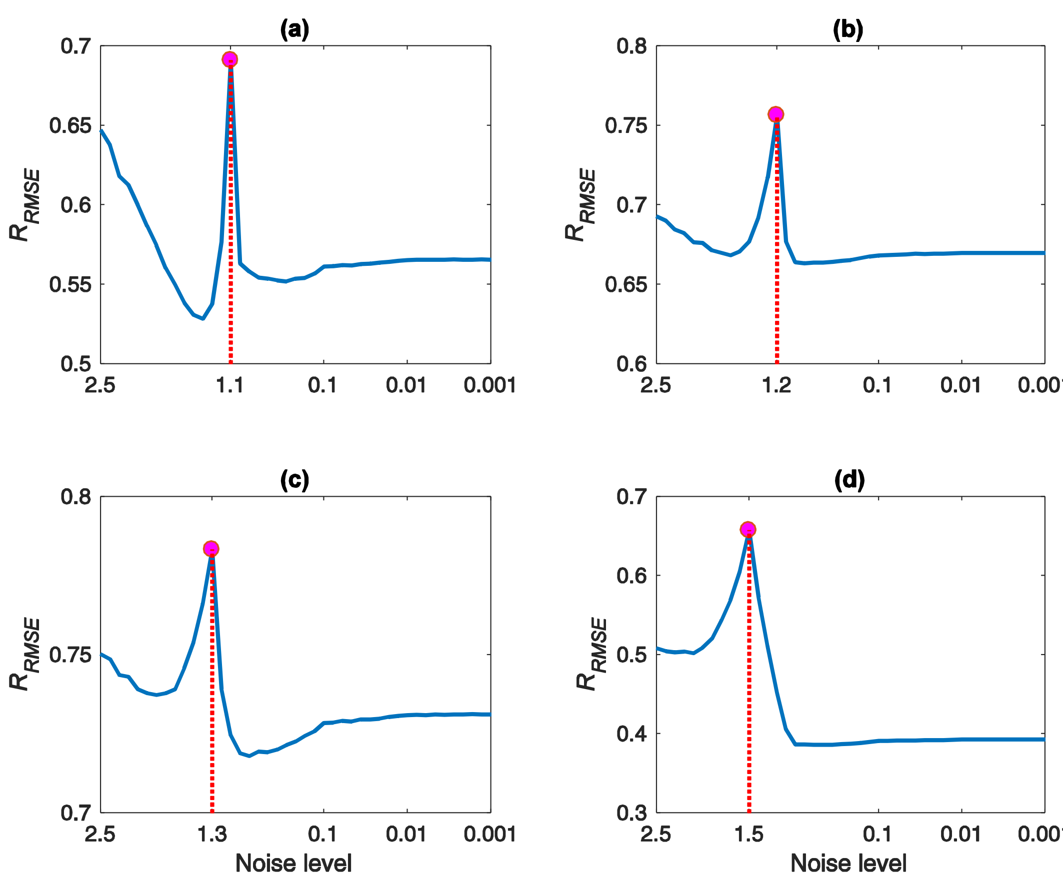

Fig. 9. Selection of the noise level for the EEMD method: (a) Sensor 7 in Case 1, (b) Sensor 12 in Case 2, (c) Sensor 5 in Case 3, (d) Sensor 4 in Case 4.

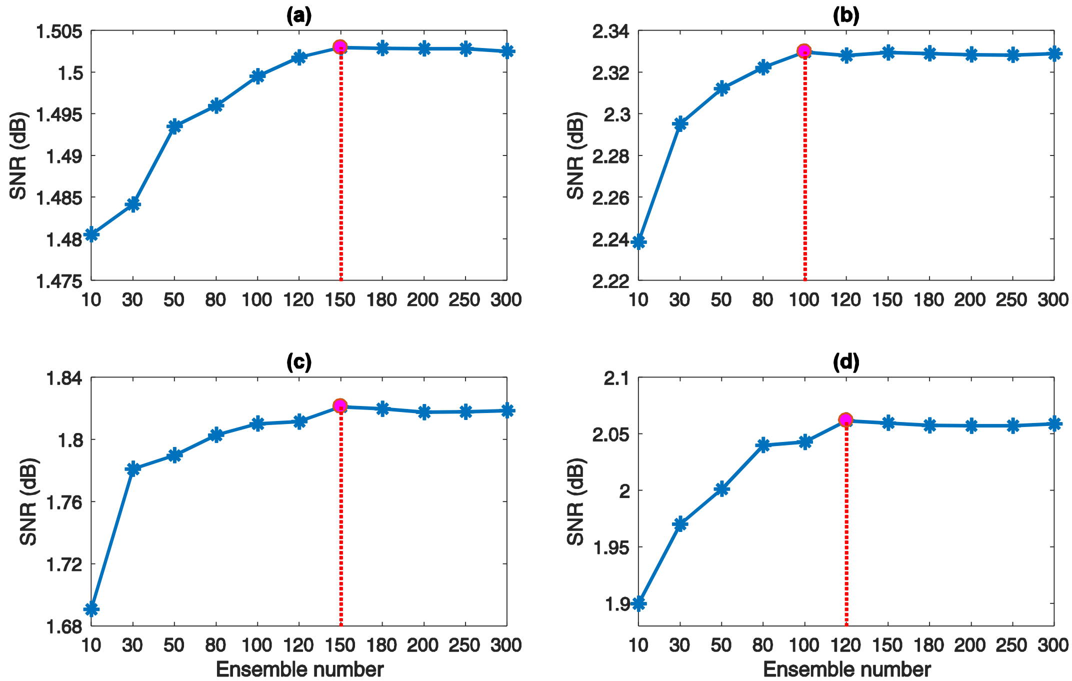

Fig. 10. Selection of the ensemble number for the EEMD method: (a) Sensor 7 in Case 1, (b) Sensor 12 in Case 2, (c) Sensor 5 in Case 3, (d) Sensor 4 in Case 4.

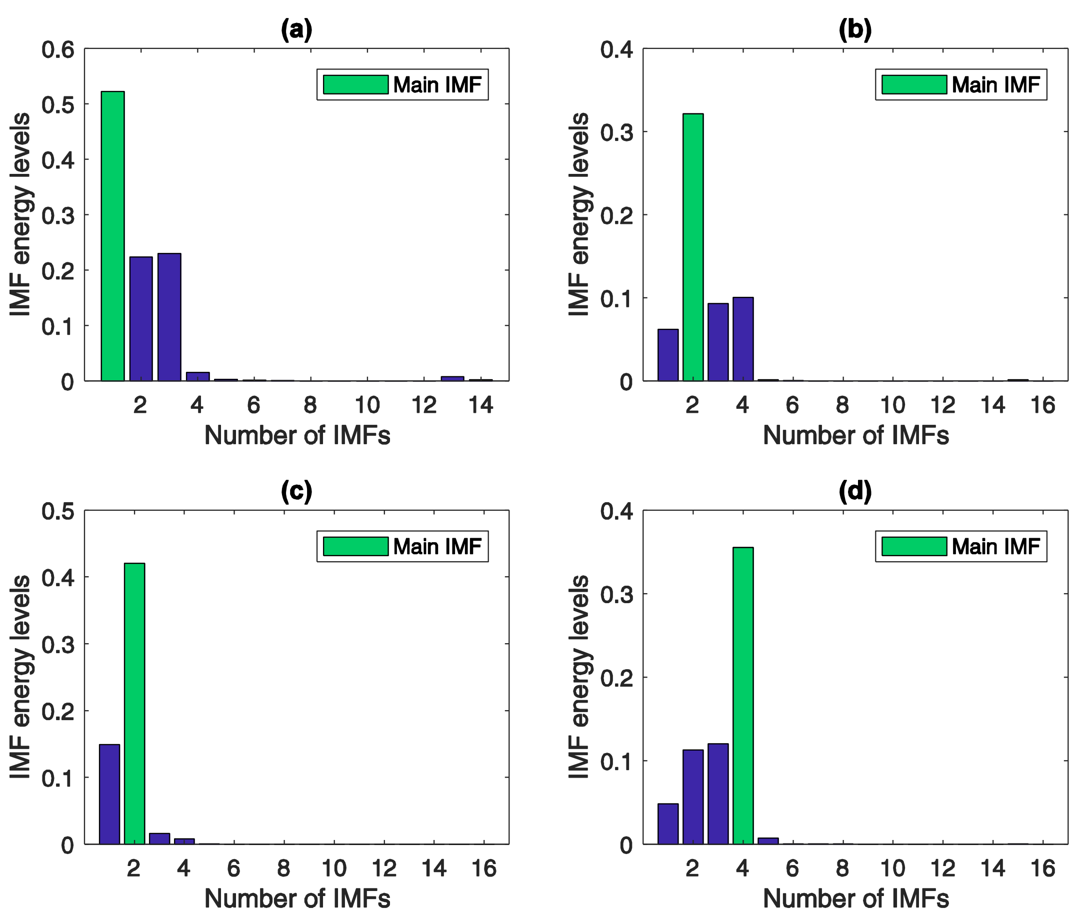

Fig. 11. The energy levels of IMFs at the sensor 15 for the: (a) Case 1, (b) Case 2, (c) Case 3, (d) Case 4.

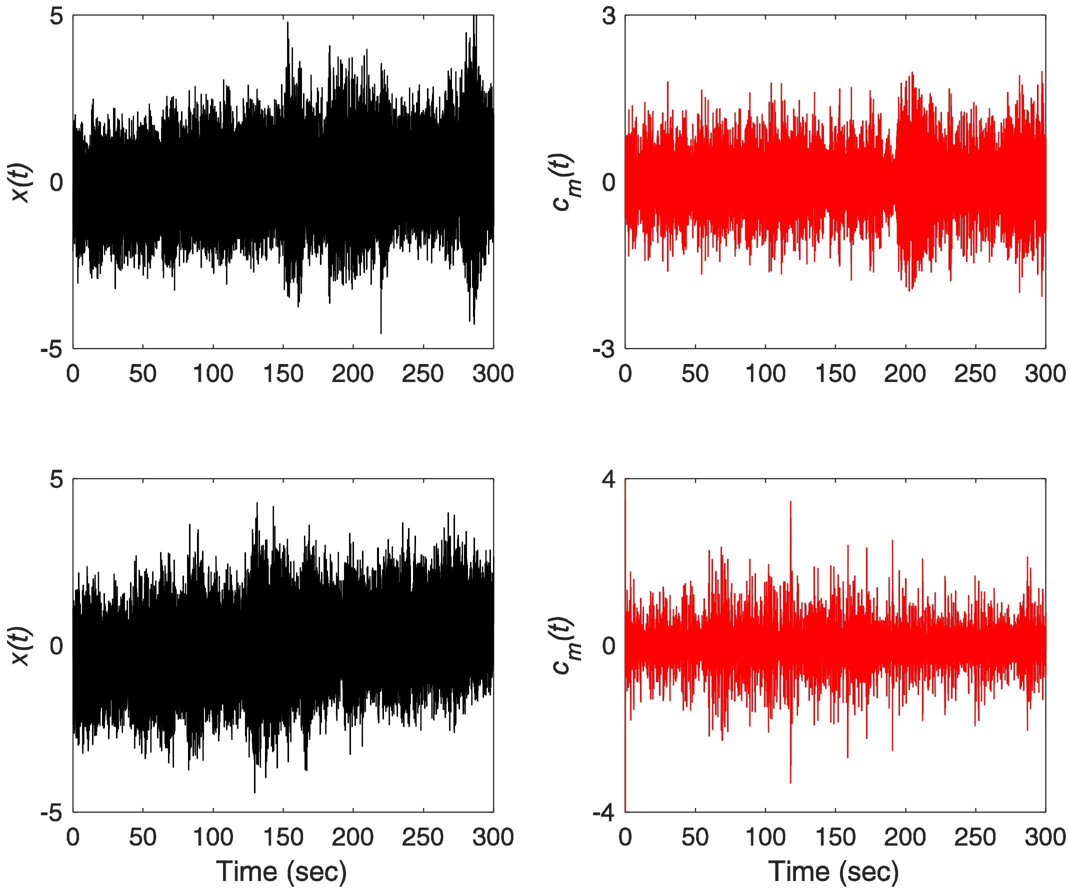

Fig. 12. Decomposition of non-stationary vibration signals (*left*) at the sensor 15 into stationary IMFs (*right*) in the cases 1 (*upper*) and 2 (*lower*).

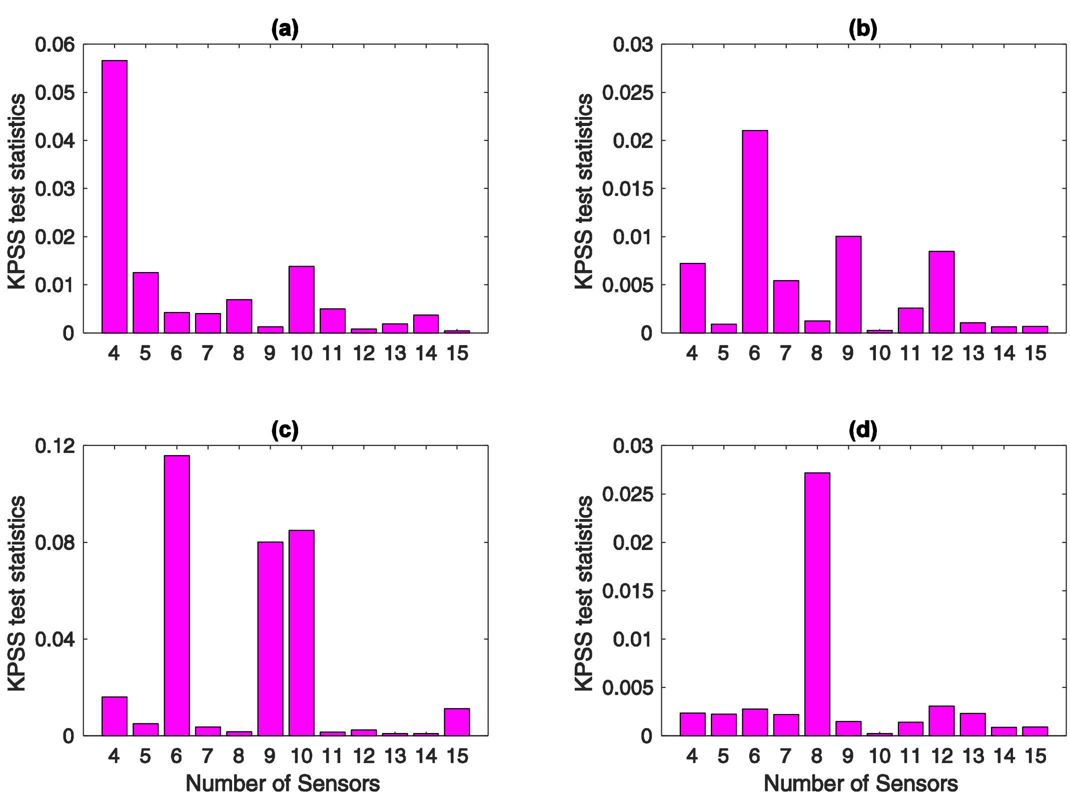

Fig. 13. Stationarity evaluation on the main IMFs using the KPSS hypothesis test: (a) Case 1, (b) Case 2, (c) Case 3, (d) Case 4.

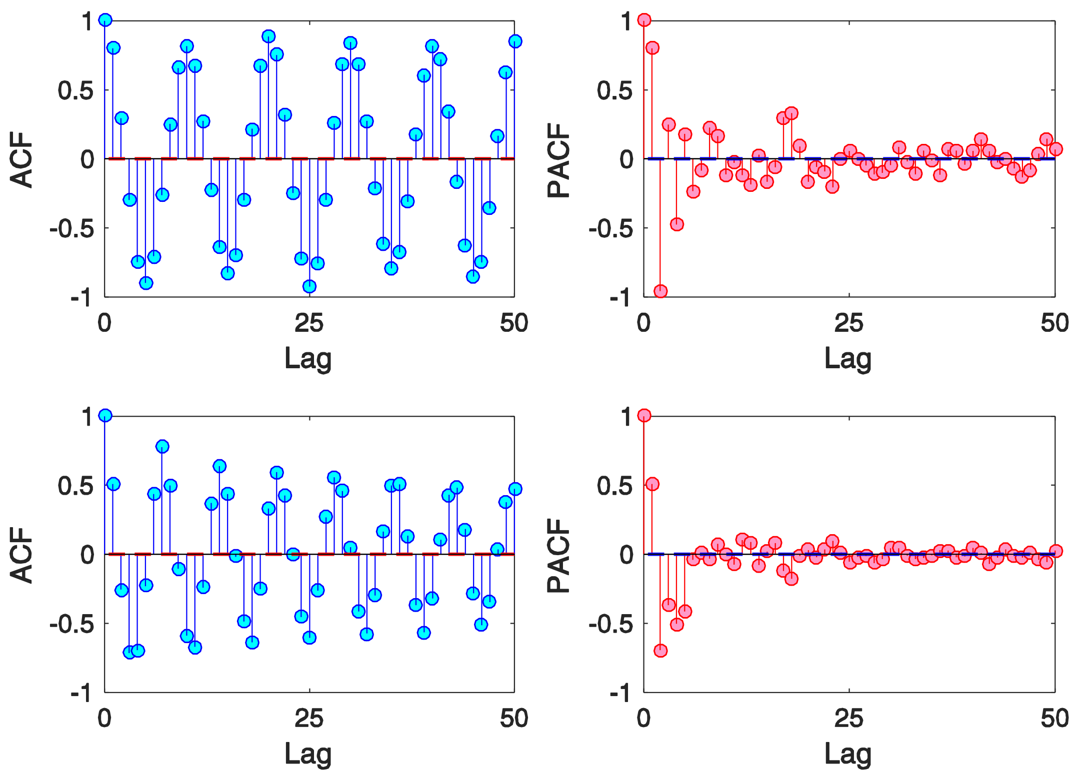

Fig. 14. The ACF (*left*) and PACF (*right*) plots of the main IMFs at the sensor 15 of the cases 1 (*upper*) 2 (*lower*).

Table 2
Determination of the AR and ARX orders by the iterative method in [24].

Sensor no.	AR		ARX	
	Order no.	*p*-value	Order no.	*p*-value
4	152	0.0609	40	0.1754
5	48	0.1255	21	0.0538
6	79	0.3495	33	0.0652
7	56	0.1446	25	0.3709
8	50	0.0594	20	0.0791
9	55	0.1877	26	0.1056
10	147	0.3072	62	0.4399
11	95	0.0716	36	0.2983
12	63	0.0738	30	0.1794
13	57	0.1341	25	0.2270
14	51	0.0756	22	0.2346
15	73	0.2382	32	0.1393

lem in the ARARX modeling when $q + r \leq p$ [29]. According to the coefficient-based feature extraction algorithm, these orders are used to estimate the AR and ARX coefficients using the least-squares technique [25]. For a comparison, Fig. 15 shows the AR coefficients of the ARX model at the sensors 8 and 15 in the cases 1–5.

It is apparent that there are no differences among the AR coefficients at the sensor 8 in Fig. 15(a), which means that this area of the IASC-ASCE structure has not been suffered from damage (i.e. removing braces). In contrast, Fig. 15(b) indicates the serious reductions in the AR coefficients due to the occurrence of damage near the sensor 15. An interesting observation in Fig. 15(b) pertains to the similarity of the AR coefficients in the cases 1 and 5. This is a reasonable result, because the braces near the sensor 15 in the fifth damage scenario were not removed from the structure. This means that the location of this sensor is the undamaged area. Finally, all observations in Fig. 15 lead to the conclusion that the AR coefficients of ARX term in the ARARX model are sensitive to damage.

In another comparison, the norm and variance of the ARX residuals in all cases are evaluated to perceive the effect of damage on the model residuals as shown in Fig. 16. From this figure, one can understand that the occurrence of damage causes increases in the residual variances and norms. In Fig. 16(a), the norms of the ARX model residuals in the healthy state are roughly inconsiderable values, whereas there are substantial increases in the damaged cases. The same conclusion is available in Fig. 16(b). Therefore, the results in Fig. 16 confirm the sensitivity of the ARX residuals to damage.

Although a simple comparison of the residual norm or variance between two different states of the structure one can distinguish a normal condition from an abnormal one, this is not a robust and reliable way to detect damage due to irregular increases in the norms and variances of the ARX residuals in some cases. The same difficulty and unreliability are available in the comparison of the AR coefficients among different structural states. As a result, it is a great necessity to use reliable and influential mathematical and/or statistical methods in the step of feature classification for detecting and locating damage.

6.5. Early damage detection and localization

To detect early damage, the ARX residuals at each sensor are collected to establish the residual matrices for the healthy and damaged conditions ($\mathbf{Z_u}$ and $\mathbf{Z_d}$). These matrices make randomly high-dimensional multivariate sets including 60,000 rows (nt) and 12 columns (ns) in five cases. Based on the CDTW method, it is initially necessary to specify the numbers of principal components (n_{PC}) and segments (υ) as described in Section 5.2. Applying the AEC approach, n_{PC} for the cases 1–4 correspond to 5 and for the case 5 is equal to 6. The results of determining the number of segments are indicated in Figs. 17 and 18 for the Hotelling's T^2 statistic

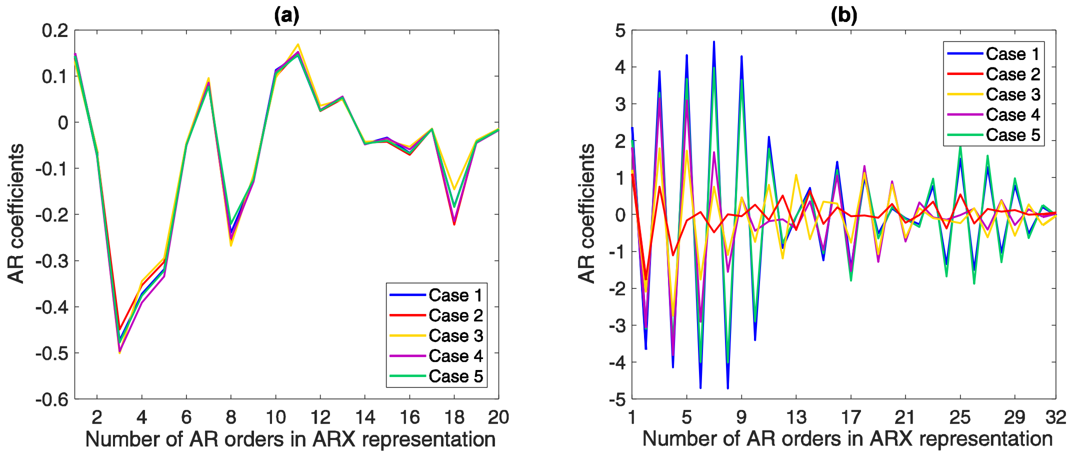

Fig. 15. Comparison of the AR coefficients in the ARX model for the cases 1–5: (a) Sensor 8, (b) Sensor 15.

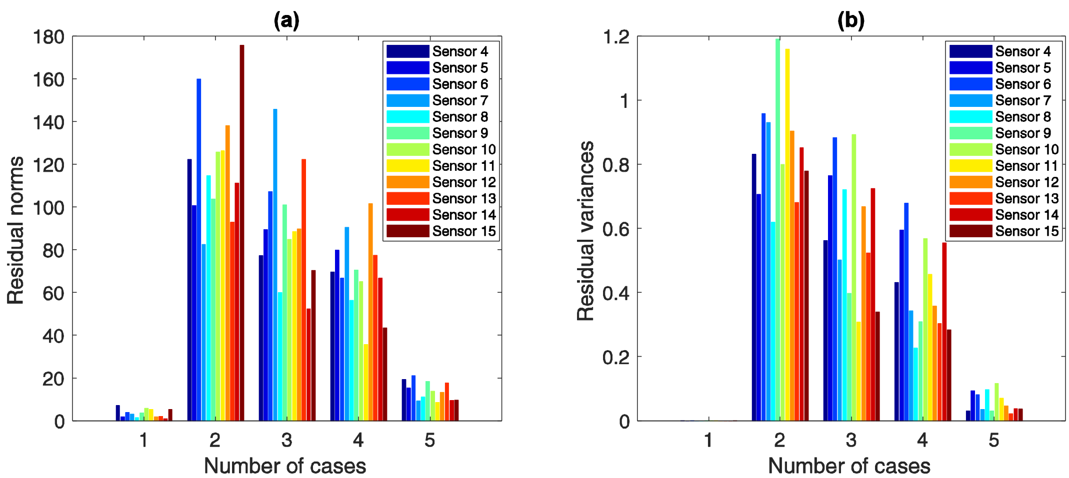

Fig. 16. Comparison of the ARX residuals of the ARARX model in the cases 1–5: (a) the residual norms, (b) the residual variances.

and QRE cost functions, respectively. From these figures, one can perceive that the increase in the number of segments leads to the reduction in ρ_r so that from the 30th segment in both Hotelling's T^2 statistic and QRE cost functions the relative reduction rates to be invariant and close to zero. Therefore, the number of segments is set as 30.

By determining the numbers of principal components and segments, $\mathbf{Z_u}$ and $\mathbf{Z_d}$ are partitioned into 30 segments ($\mathbf{S_u}$ and $\mathbf{S_d}$), each of which consists of five (for the cases 1–4) and six (for the case 5) principal components. Finally, the CDTW dissimilarity quantity using PCA similarity factor is used to detect early damage. Fig. 19 illustrates the results of early damage detection for both Hotelling's T^2 and QRE cost functions.

It can be observed that the *DS* quantities correspond to zero in the case 1, when there is no damage in the IASC-ASCE structure. During the occurrence of damage, the *DS* value deviates from the normal condition as shown in the *DS* quantities of the cases 2–5. As Fig. 19 appears, the largest *DS* value belongs to the second case, where the braces of all floors were removed from the east side of the structure. Hence, this case is equivalent to the highest level of damage severity. By contrast, the smallest *DS* quantity occurs in the case 5, for which the braces of the first story were only eliminated from the southeast corner. This means that the lowest damage level belongs to the fifth case. These observations confirm that the CDTW method is not only able to detect early damage but also estimate the level of damage severity. Furthermore, due to the reliable results obtained from this method in conjunction with the proposed EEMD-ARARX algorithm, one can conclude that the unmeasurable and unknown ambient excitations do not have any effects on the early damage detection and quantification.

To locate damage in the cases 2–5, the AR coefficients of ARX representation in the ARARX model ($\mathbf{\Phi_u}$ and $\mathbf{\Phi_d}$) obtained from 12 sensors are used in the DTW method to establish a damage localization vectors (**DLV**) for each damage scenario. Using 5% significant limit, a threshold value is calculated for each case based on Eq. (21). The results of damage localization are illustrated in Fig. 20, where the dashed blue arrows show the threshold amounts. Furthermore, "DL" means the damaged location and "UDL" implies the undamaged area.

In Fig. 20(a) and (b), the DTW quantities of sensors 6, 9, 12, and 15 exceed the threshold limits implying the damage locations. For the case 4 in Fig. 20(c), the locations of sensors 6 and 15 are identified as the damaged areas in the IASC-ASCE structure. Eventually, as Fig. 20(d) shows, the only DTW value of the sensor 6 is more than the threshold value indicating the location of single damage. Based on Fig. 2(b) and Table 1, one can realize that all observations in Fig. 20 give reasonable and accurate damage localization results. Due to the removal of braces from all floors of the east side of the IASC-ASCE structure, the locations of sensors 6, 9, 12, and 15 were situated near the damaged area in the cases 2 and 3. Furthermore, the elimination of braces from the first and fourth floors at the southeast corner occurred at the sensors 6 and 15 in the case 4.

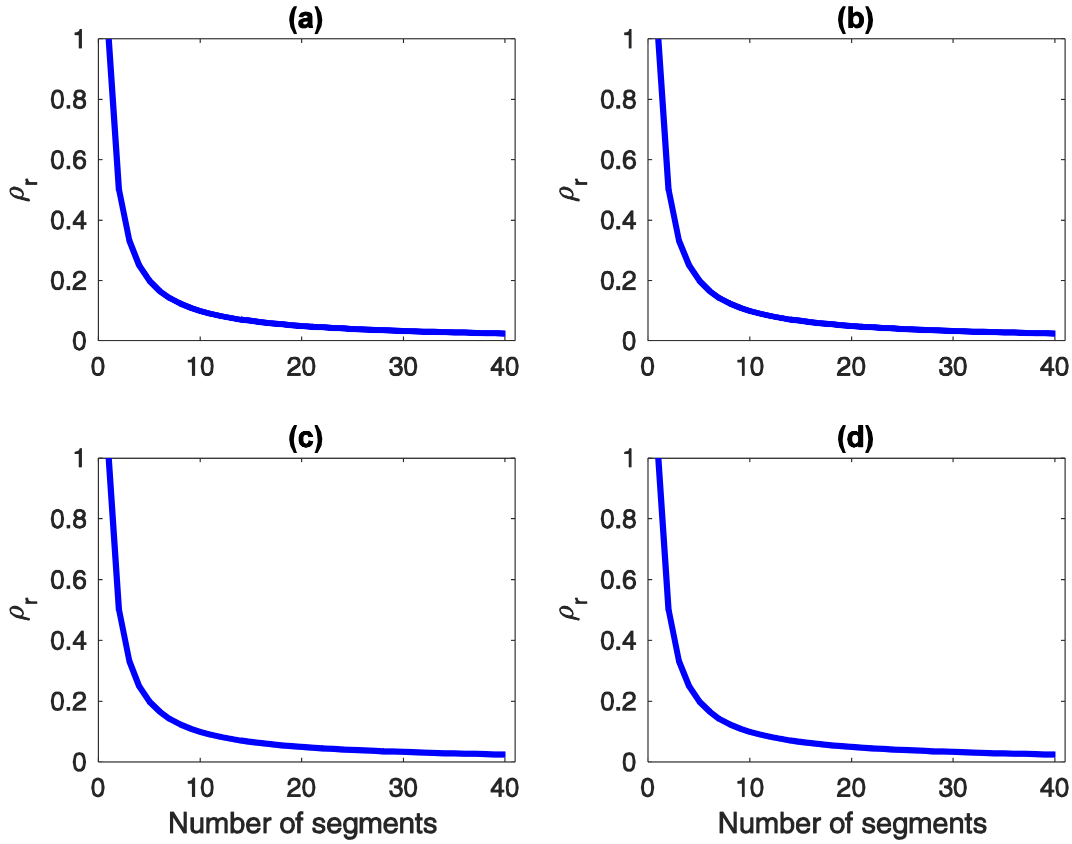

Fig. 17. The relative reduction rates of the Hotelling's T^2 statistic: (a) Case 2, (b) Case 3, (c) Case 4, (d) Case 5.

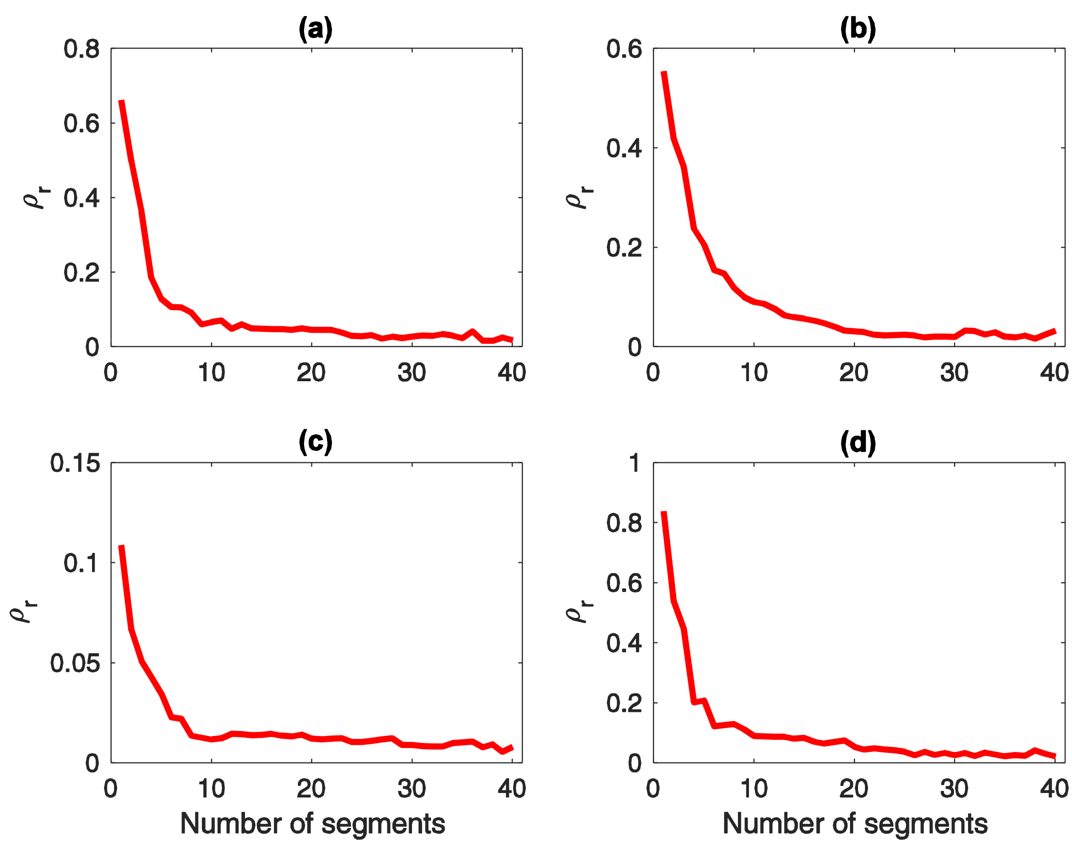

Fig. 18. The relative reduction rates of the QRE: (a) Case 2, (b) Case 3, (c) Case 4, (d) Case 5.

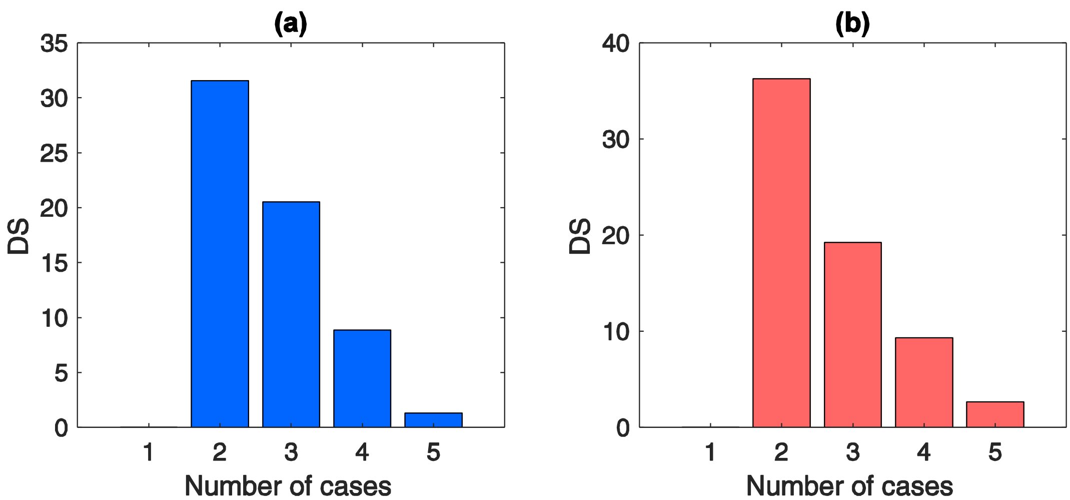

Fig. 19. Early damage detection via the CDTW method by using the ARX residuals of the ARARX model: (a) Hotelling's T^2 statistic, (b) QRE.

Eventually, the only sensor 6 was located near the damaged area in the case 5. Therefore, it can be seen in Fig. 20 that the DTW method is precisely able to locate the single (case 5) and multiple (cases 2–4) damage scenarios from a relatively dense sensor network. On this basis, the sensor location associated with the largest DTW value that exceeds the threshold limit is identified as the damaged area.

For further assessment, it is attempted to compare the superiority of the proposed EEMD-ARARX algorithm to the conventional EMD-AR approach [31,32] for the problems of early damage detection and localization. Similar to the proposed hybrid algorithm, all IMFs of each vibration signal are initially extracted from the EMD technique. Subsequently, the main IMF is chosen to use in the AR modeling. In this regard, the AR model coefficients and residuals are extracted as the DSFs. Fig. 21 shows the results of early damage detection by using the proposed CDTW method and the EMD-AR algorithm.

With regard to the great ability of the CDTW method to detect early damage by using the randomly high-dimensional data, one can observe in Fig. 21 that the features extracted from the EMD-AR algorithm can discriminate the normal condition from the damaged states. However, a simple comparison between the EEMD-ARARX (Fig. 19) and EMD-AR algorithms (Fig. 21) reveals that the latter fails in quantifying the level of damage severity. To prove this conclusion in an analytical manner, one can compare the rate of increase (the percentage increase) in the DS values gained by the DSFs extracted from the EEMD-ARARX and EMD-AR algorithms. For this comparison, it is only necessary to calculate the relative errors in the DS quantities between the smallest damage scenario (case 5) and the other damaged cases as listed in Table 3. Note that since the DS values associated with the Hotelling's T^2 and QRE cost functions are roughly similar, the distance quantities gained by the QRE are used in the comparison procedure.

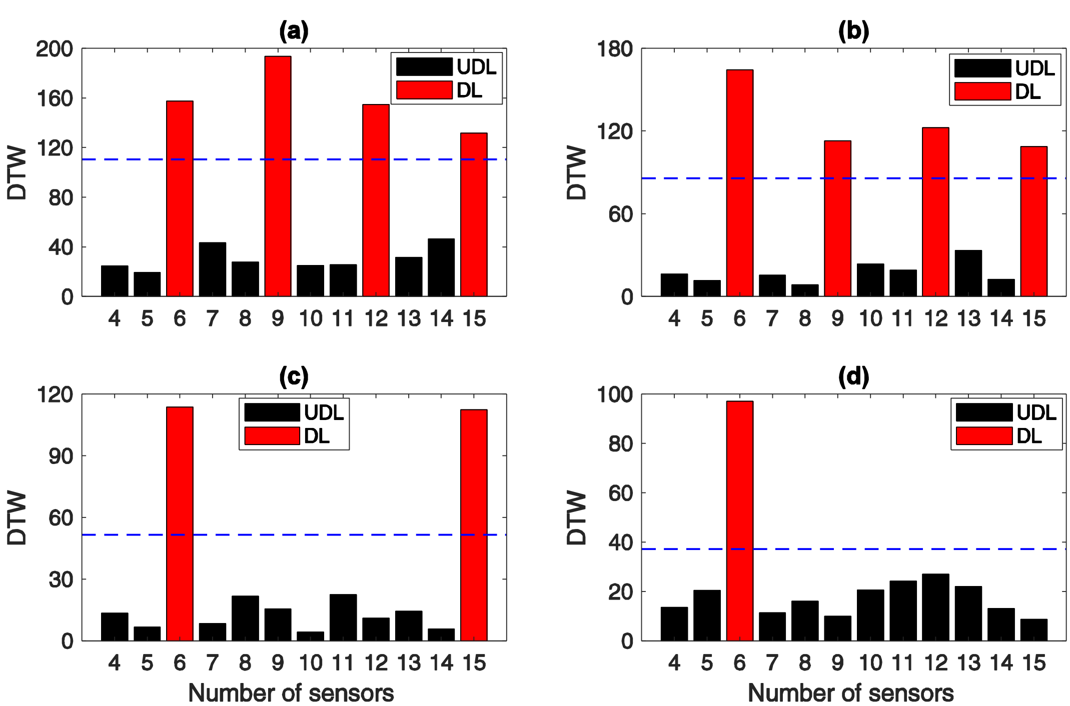

Fig. 20. Damage localization via the DTW method by using the AR coefficients of the ARX representation in the ARARX model: (a) Case 2, (b) Case 3, (c) Case 4, (d) Case 5.

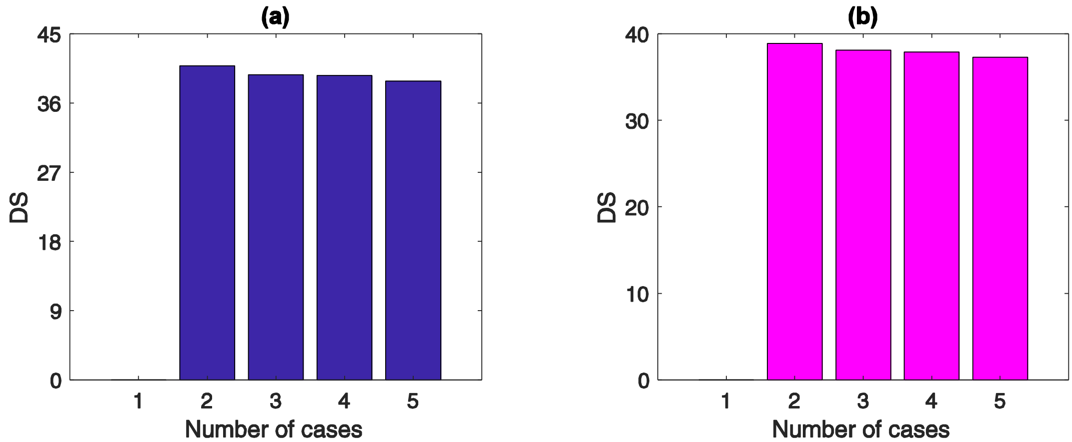

Fig. 21. Early damage detection via the CDTW method by using the AR residuals based on the EMD-AR algorithm: (a) Hotelling's T^2 statistic, (b) QRE.

Table 3
The percentage increases in the DS values based on the EEMD-ARARX and EMD-AR algorithms between the case 5 and the cases 2–4.

Algorithm	Case no.			
	2	3	4	5
EEMD-ARARX	92.67%	86.21%	71.64%	0%
EMD-AR	4.11%	2.10%	1.56%	0%

The amounts in Table 3 reveal that there are large increases in the relative errors (the percentage increases) of the DS values obtained from the proposed EEMD-ARARX algorithm between the case 5 and the cases 2–4. In contrast, it is apparent that the percentages of the relative errors in the DS quantities gained by the EMD-AR algorithm for the cases 2–4 are very close to the case 5. An important note is that the DS values based on both the EEMD-ARARX and EMD-AR algorithms (see Fig. 19(b) and 21(b)) roughly vary in the same amounts ($0 < DS < 40$). However, the percentage increases in the EMD-AR algorithm is not as good as the EEMD-ARARX approach. As a result, it is deduced that the conventional EMD-AR algorithm does not appropriately enable the CDTW method to estimate the level of damage severity.

Fig. 22 illustrates the results of damage localization by the DTW method based on the AR coefficients extracted from the EMD-AR algorithm. From this figure, it is apparent that there are erroneous and unreliable results of locating the structural damages in all cases. This is because of the false identification of the undamaged areas of the structure as the damage locations (false positive) and serious errors in locating the actual damages (false negative). Such erroneous results may be due to the influence of ambient excitations, the poor performance of AR representation for modeling the vibration signals or IMFs caused by the ambient vibration, and the problem of mode mixing in the EMD technique. For more evaluation, Table 4 lists the percentages of the false positives (Type I errors) and false negatives (Type II errors) in the process of dam-

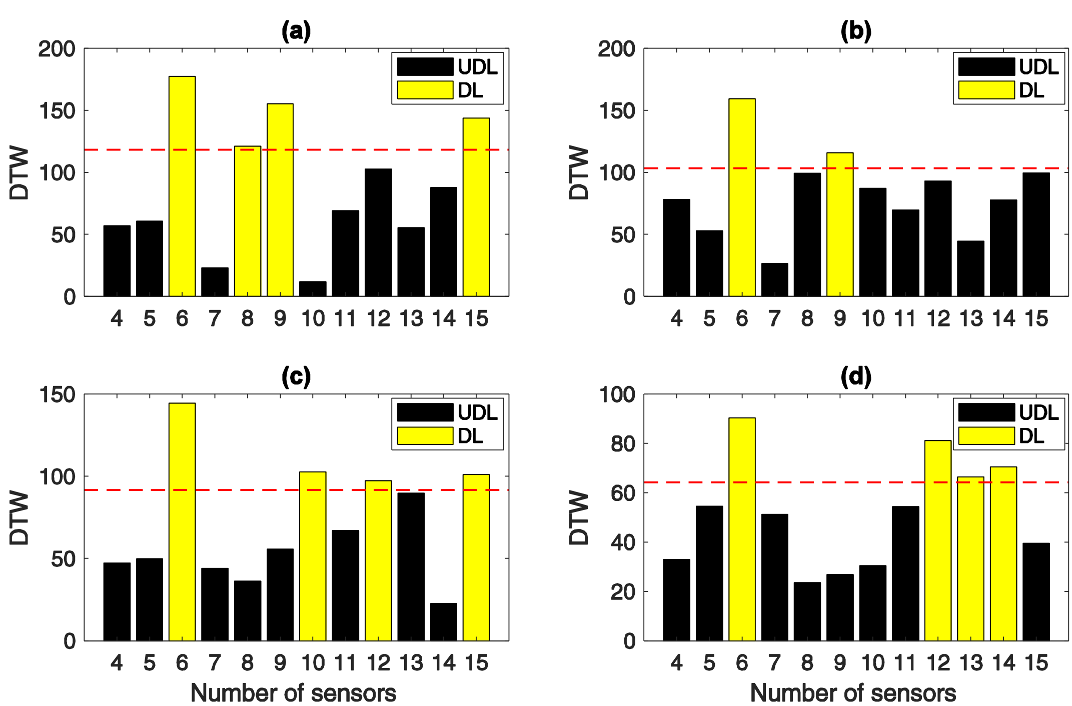

Fig. 22. Damage localization via the DTW method by using the AR coefficients based on the EMD-AR algorithm: (a) Case 2, (b) Case 3, (c) Case 4, (d) Case 5.

Table 4
Type I and Type II errors in the damage localization based on the EMD-AR algorithm.

Error	Case no.			
	2	3	4	5
Type I	8.34%	0%	8.34%	25%
Type II	8.34%	16.67%	8.34%	0%
Total	16.67%	16.67%	16.67%	25%

age localization based on the EMD-AR algorithm. In the context of SHM, a Type I error means that the structure is undamaged but the decision-making system alarms the occurrence of damage, whereas a Type II error refers to a situation that the structure suffers from damage but the decision-making system does not alarm the occurrence of damage [43].

Unlike the proposed EEMD-ARARX algorithm, for which both the Type I and Type II errors are zero (see Fig. 20), there are relatively large errors in the results of the EMD-AR algorithm. Therefore, one can conclude that the proposed EEMD-ARARX algorithm provides better DSFs than the EMD-AR algorithm for the localization of damage under the ambient excitation and non-stationary/stationary vibration signals.

7. Conclusions

In order to extract the significant DSFs from the non-stationary vibration signals under ambient excitations, a hybrid algorithm has been proposed as the combination of EEMD technique and ARARX model. In this algorithm, the vibration signals have initially been decomposed into several IMFs by the EEMD technique and the main IMF with the highest energy level has been chosen to use in the time series modeling. Fitting the ARARX model to this IMF, the AR coefficients and ARX residuals have been selected as the DSFs. The CDTW method based on the PCA-based segmentation techniques has been presented to detect early damage using the ARX residuals as the randomly high-dimensional multivariate data sets. To locate damage via the AR coefficients, the DTW method along with a threshold limit has been introduced. The experimental datasets of the well-known IASC-ASCE benchmark structure have been utilized to validate the accuracy and reliability of the proposed methods.

The results demonstrated that the proposed EEMD-ARARX algorithm is an efficient and reliable tool for extracting the reliable DSFs from the non-stationary and/or stationary vibration signals acquired from the ambient excitations. In particular, when the nature of vibration signals is unknown or unpredictable, the proposed algorithm is an appropriate and robust choice. The comparison of the AR coefficients and ARX residuals of the ARARX model between the different structural cases was shown that these features are properly sensitive to damage. For the early damage detection, the CDTW method with the aid of the PCA-based segmentation techniques dealt with the limitation of using high-dimensional features. The results confirmed that the CDTW dissimilarity quantity based on PCA similarity factor is not only able to detect damage, but also estimate the level of damage severity. Accordingly, the normal condition has a dissimilarity value close to zero and any deviation from the normal state is indicative of damage occurrence. In the process of damage localization, it was seen that the DTW method using the AR coefficients precisely identified the locations of single and multiple damage cases. On this basis, the sensor location associated with the largest DTW quantity more than the threshold limit is identified as the damaged area. Eventually, the comparison of the proposed EEMD-ARARX algorithm with the EMD-AR approach in the problems of early damage detection, localization, and quantification revealed that the proposed method provides better and more reliable DSFs than the EMD-AR algorithm under the ambient excitations and non-stationary and/or stationary vibration signals.

Acknowledgments

This research was supported by a Grant No. 96007230 from the Iran National Science Foundation (INSF). The authors would like to express their sincere gratitude to ASCE Structural Health Monitoring Task Group for the experimental datasets of the four-story steel structure.

References

[1] C.R. Farrar, K. Worden, An introduction to structural health monitoring, Philos. Trans. R. Soc. A 2007 (365) (1851) 303–315.
[2] T.-H. Yi, H.-B. Huang, H.-N. Li, Development of sensor validation methodologies for structural health monitoring: a comprehensive review, Measurement 109 (2017) 200–214.
[3] A. Cunha et al., Recent perspectives in dynamic testing and monitoring of bridges, Struct. Control Health Monitoring 20 (6) (2013) 853–877.
[4] H. Hashim, Z. Ibrahim, H.A. Razak, Dynamic characteristics and model updating of damaged slab from ambient vibration measurements, Measurement 46 (4) (2013) 1371–1378.
[5] J.P. Amezquita-Sanchez, H. Adeli, Signal processing techniques for vibration-based health monitoring of smart structures, Arch. Comput. Methods Eng. 23 (1) (2016) 1–15.
[6] Y. Lei et al., A review on empirical mode decomposition in fault diagnosis of rotating machinery, Mech. Syst. Sig. Process. 35 (1) (2013) 108–126.
[7] Z. Feng, M. Liang, F. Chu, Recent advances in time–frequency analysis methods for machinery fault diagnosis: a review with application examples, Mech. Syst. Sig. Process. 38 (1) (2013) 165–205.
[8] K. Worden et al., Some recent developments in SHM based on nonstationary time series analysis, Proc. IEEE 104 (8) (2016) 1589–1603.
[9] W.J. Staszewski, A.N. Robertson, Time–frequency and time–scale analyses for structural health monitoring, Philos. Trans. R. Soc. London A 2007 (365) (1851) 449–477.
[10] N.E. Huang et al., The empirical mode decomposition and the Hilbert spectrum for nonlinear and non-stationary time series analysis, Proceedings of the Royal Society of London A: Mathematical, Physical and Engineering Sciences, The Royal Society, 1998.
[11] Z. Wu, N.E. Huang, Ensemble empirical mode decomposition: a noise-assisted data analysis method, Adv. Adaptive Data Anal. 1 (1) (2009) 1–41.
[12] W. Guo, W.T. Peter, A. Djordjevich, Faulty bearing signal recovery from large noise using a hybrid method based on spectral kurtosis and ensemble empirical mode decomposition, Measurement 45 (5) (2012) 1308–1322.
[13] X. Zhang, Y. Liang, J. Zhou, A novel bearing fault diagnosis model integrated permutation entropy, ensemble empirical mode decomposition and optimized SVM, Measurement 69 (2015) 164–179.
[14] C. Yang, T. Wu, Diagnostics of gear deterioration using EEMD approach and PCA process, Measurement 61 (2015) 75–87.
[15] X.-H. Chen et al., Research of weak fault feature information extraction of planetary gear based on ensemble empirical mode decomposition and adaptive stochastic resonance, Measurement 73 (2015) 55–67.
[16] G. Cheng et al., Study on planetary gear fault diagnosis based on entropy feature fusion of ensemble empirical mode decomposition, Measurement 91 (2016) 140–154.
[17] H. Aied, A. González, D. Cantero, Identification of sudden stiffness changes in the acceleration response of a bridge to moving loads using ensemble empirical mode decomposition, Mech. Syst. Sig. Process. 66 (2016) 314–338.
[18] Y. Kim et al., System identification of smart buildings under ambient excitations, Measurement 87 (2016) 294–302.
[19] H. Zheng, A. Mita, Localized damage detection of structures subject to multiple ambient excitations using two distance measures for autoregressive models, Struct. Health Monitoring 8 (3) (2009) 207–222.
[20] A.A. Mosavi et al., Identifying damage locations under ambient vibrations utilizing vector autoregressive models and Mahalanobis distances, Mech. Syst. Sig. Process. 26 (2012) 254–267.
[21] M. Gul, F.N. Catbas, Damage assessment with ambient vibration data using a novel time series analysis methodology, J. Struct. Eng. 137 (12) (2010) 1518–1526.
[22] E.P. Carden, J.M. Brownjohn, ARMA modelled time-series classification for Structural Health Monitoring of civil infrastructure, Mech. Syst. Sig. Process. 22 (2) (2008) 295–314.
[23] Q. Zhang, Statistical damage identification for bridges using ambient vibration data, Comput. Struct. 85 (7) (2007) 476–485.
[24] A. Entezami, H. Shariatmadar, An unsupervised learning approach by novel damage indices in structural health monitoring for damage localization and quantification, Struct. Health Monitoring (2017) 0(0).
[25] G.E. Box et al., Time Series Analysis: Forecasting and Control, 5th ed., John Wiley & Sons, 2015.

[26] F.N. Catbas, M. Malekzadeh, A machine learning-based algorithm for processing massive data collected from the mechanical components of movable bridges, Autom. Constr. 72 (2016) 269–278.
[27] X. Wang et al., Experimental comparison of representation methods and distance measures for time series data, Data Min. Knowl. Disc. 26 (2) (2013) 275–309.
[28] W. Guo, W.T. Peter, A novel signal compression method based on optimal ensemble empirical mode decomposition for bearing vibration signals, J. Sound Vib. 332 (2) (2013) 423–441.
[29] L. Ljung, System Identification: Theory for the User, 2nd ed., Prentice-Hall, Upper Saddle River, NJ, 1999.
[30] M. Rezaiee-Pajand, A. Entezami, H. Shariatmadar, An iterative order determination method for time-series modeling in structural health monitoring, Adv. Struct. Eng. (2017).
[31] C. Junsheng, Y. Dejie, Y. Yu, A fault diagnosis approach for roller bearings based on EMD method and AR model, Mech. Syst. Sig. Process. 20 (2) (2006) 350–362.
[32] F. Li, B. Tang, R. Yang, Rotating machine fault diagnosis using dimension reduction with linear local tangent space alignment, Measurement 46 (8) (2013) 2525–2539.
[33] S. Adwan, I. Alsaleh, R. Majed, A new approach for image stitching technique using Dynamic Time Warping (DTW) algorithm towards scoliosis X-ray diagnosis, Measurement 84 (2016) 32–46.
[34] S. Adwan, H. Arof, On improving Dynamic Time Warping for pattern matching, Measurement 45 (6) (2012) 1609–1620.
[35] T. Han, X. Liu, A.C.C. Tan, Fault diagnosis of rolling element bearings based on Multiscale Dynamic Time Warping, Measurement 95 (2017) 355–366.
[36] C. Bao, H. Hao, Z.-X. Li, Integrated ARMA model method for damage detection of subsea pipeline system, Eng. Struct. 48 (2013) 176–192.
[37] Z. Bankó, J. Abonyi, Correlation based dynamic time warping of multivariate time series, Expert Syst. Appl. 39 (17) (2012) 12814–12823.
[38] W. Krzanowski, Between-groups comparison of principal components, J. Am. Stat. Assoc. 74 (367) (1979) 703–707.
[39] S.J. Dyke et al., Experimental phase II of the structural health monitoring benchmark problem, Proceedings of the 16th ASCE engineering mechanics conference, 2003.
[40] L. Kirkup, R.B. Frenkel, An introduction to uncertainty in measurement: using the GUM, Cambridge University Press, 2006.
[41] C. Ratcliffe, B. Ratcliffe, Doubt-Free Uncertainty in Measurement: An Introduction for Engineers and Students, Springer, 2014.
[42] D. Kwiatkowski et al., Testing the null hypothesis of stationarity against the alternative of a unit root, J. Econ. 54 (1992) 159–178.
[43] L. Balsamo, R. Betti, H. Beigi, A structural health monitoring strategy using cepstral features, J. Sound Vib. 333 (19) (2014) 4526–4542.